# Delayed activation of the DNA replication licensing system in Lgr5(+) intestinal stem cells

T.D. Carroll[1], I.P. Newton[1], J.J. Blow*[2], I.Näthke*[1]

Affiliations: [1]Cell & Developmental Biology and [2]Centre for Gene Regulation and Expression, University of Dundee, Dundee, Scotland, UK, DD15EH
*Correspondence to: j.j.blow@dundee.ac.uk or i.s.nathke@dundee.ac.uk

**ABSTRACT**

During late mitosis and early $G_1$, replication origins are licensed for replication by binding to MCM2-7 double hexamers. This signals proliferative fate commitment. Here, we investigate how licensing and proliferative commitment are coupled in the small-intestinal epithelium. We developed a method for identifying cells in intestinal crypts that contain DNA-bound MCM2-7 and are licensed for replication. Interphase cells at the top of the transit amplifying zone did not contain DNA-bound MCM2-7, but still expressed MCM2-7 protein. This suggests licensing is inhibited immediately at terminal differentiation, after a final mitosis. Strikingly, we found that at the crypt base the majority of Lgr5(+) intestinal stem cells reside in an unlicensed state, despite expressing MCM2-7 protein and the Ki67 proliferation marker. This state, which we call 'shallow-$G_0$', might allow stem cells to be easily activated to re-enter the cell cycle. We demonstrate that the dynamics of the licensing system provides a novel means to assess the unique cell-cycle of intestinal epithelial cells.

**Delayed activation of the DNA replication licensing system in Lgr5(+) intestinal stem cells**

## INTRODUCTION

Cell division is necessary for adult tissue homeostasis. It allows for the replacement of aged or damaged cells and the provision of specialised cells critical for tissue function. The decision to proliferate is crucial, especially for stem cells which produce daughter cells that either maintain a stem cell fate or differentiate to produce specialised cells. The rapidly-renewing intestinal epithelium replenishes its cellular content every 4-5 days. This high turnover rate is maintained primarily by Lgr5(+) intestinal stem cells in the crypt base, thought to be continually proliferative (Basak et al., 2014) as confirmed by proteomic and transcriptomic analysis (Munoz et al., 2012). There is also a quiescent stem cell-population that can re-engage with the cell-cycle to repopulate the Lgr5(+) cell population if it becomes depleted. These quiescent stem cells reside at the +4 position and constitute a subset of Lgr5(+) cells and are immature secretory lineage precursors (Buczacki et al., 2013). Lgr5(+) stem cells can divide to form transit-amplifying (TA) cells, which undergo several rounds of cell division before differentiating and losing proliferative competency (Potten and Loeffler, 1990).

How proliferative fate decisions are governed in stem cells and transit-amplifying cells is not understood. Lineage tracing studies suggest that in homeostatic intestinal tissue only 5-7 intestinal stem cells are ‘active’ out of the 12-16 Lgr5(+) cells present in the crypt base (Baker et al., 2014, Kozar et al., 2013). Interestingly, Lgr5(+) cells have a significantly longer cell-cycle than transit-amplifying cells (Schepers et al., 2011). The functional significance of the prolonged cell-cycle time of Lgr5(+) stem cells is currently unknown, but suggests active regulation of cell-cycle progression and proliferative fate commitment.

**Delayed activation of the DNA replication licensing system in Lgr5(+) intestinal stem cells**

43 Proliferative fate decisions are typically visualised by detecting markers that are present in
44 all cell-cycle phases, and only distinguish proliferative from quiescent cells. Visualising the
45 incorporation of labelled nucleosides such as BrdU or EdU marks cells in S-phase. The
46 limitation of these methods is that they cannot discriminate early proliferative fate
47 decisions made during the preceding mitosis, or in the early stages of $G_1$. DNA replication in
48 S phase depends on origins having been licensed, which involves the regulated loading of
49 minichromosome maintenance 2-7 (MCM2-7) complexes onto origins of DNA replication
50 (reviewed in (Champeris Tsaniras et al., 2014)). During S phase, DNA-bound MCM2-7
51 hexamers are activated to form the catalytic core of the DNA helicase as part of the CMG
52 (Cdc45, MCM2-7, GINS) complex (Moyer et al., 2006, Ilves et al., 2010, Makarova et al.,
53 2012). Replication licensing is thought to occur from late mitosis throughout $G_1$ until
54 passage through the restriction point (Dimitrova et al., 2002, Haland et al., 2015, Namdar
55 and Kearsey, 2006, Symeonidou et al., 2013). Correspondingly, insufficient origin licensing
56 directly limits the ability to progress past the restriction point causing cell cycle arrest (Alver
57 et al., 2014, Liu et al., 2009, Shreeram et al., 2002).

58 When cells enter $G_0$, MCM2-7 proteins are transiently downregulated and degraded,
59 primarily via E2F-mediated transcriptional control of MCM2-7, Cdc6 and Cdt1 (Leone et al.,
60 1998, Ohtani et al., 1999, Williams et al., 1998). This prevents terminally differentiated cells
61 from re-entering the cell cycle. In mammalian cells, artificial induction of quiescence
62 through contact inhibition leads to gradual downregulation of Cdc6 and MCM2-7 over
63 several days (Kingsbury et al., 2005). These features have led to the suggestion that
64 quiescence can be defined by being an unlicensed state (Blow and Hodgson, 2002). Equally,
65 the licensing status can define a different restriction point that signals proliferative fate

66 commitment at the end of mitosis and in early $G_1$, independently of the Rb/E2F restriction
67 point.

68 The dynamics of replication licensing in the intricate cellular hierarchy of a complex, rapidly
69 renewing adult tissue, is not understood. We therefore investigated the licensing system in
70 the intestinal epithelium, aiming to understand dynamics of early cell-cycle commitment in
71 stem and transit-amplifying cells and during terminal differentiation.

72 **MATERIALS AND METHODS**

73 **Mice**

74 All experiments were performed under UK home office guidelines. CL57BL/6 (Wild-type),
75 *R26-rtTA Col1A1-H2B-GFP* (H2B-GFP), Lgr5-EGFP-IRES-creERT2 ($Lgr5^{GFP/+}$) and $Apc^{Min/+}$ mice
76 were sacrificed by cervical dislocation or $CO_2$ asphyxiation.

77 **Tissue preparation: Whole small intestine**

78 Dissected pieces of adult mouse small-intestine were washed briefly in PBS and then fixed in
79 4% PFA for 3 hours, 4°C. Intestines were cut into 2x2 $cm^2$ pieces and fixed overnight in 4%
80 PFA, 4°C. Tissue was embedded in 3% low melting temperature agarose and cut into 200 µm
81 sections using a Vibratome (Leica). Sections were washed in PBS, permeabilised with 2%
82 Triton-X100 for 2 hours and incubated with Blocking Buffer (1% BSA, 3% Normal Goat
83 serum, 0.2% Triton-X100 in PBS) for 2 hours, 4°C. Tissue was incubated in Working Buffer
84 (0.1% BSA, 0.3% Normal Goat Serum, 0.2% Triton-X100 in PBS) containing primary antibody,
85 Mcm2 (Cell Signalling, 1:500), for 48 hours, 4°C. Sections were washed 5x with Working
86 Buffer prior to 48 hour incubation with secondary antibodies diluted in Working Buffer:

87 Alexafluor™ conjugated goat anti-rabbit (1:500, Molecular Probes) plus 5 µg/ml Hoechst
88 33342 and Alexafluor™ conjugated Phalloidin (1:150, Molecular Probes). Sections were
89 mounted on coverslips in Prolong Gold between 2x120 µm spacers.

90 **Tissue preparation: Isolated Crypts**

91 Small intestines were dissected, washed in PBS and opened longitudinally. Villi were
92 removed by sequential scraping of the luminal surface with a coverslip. Tissue was washed
93 in PBS, incubated in 30 mM EDTA (25 minutes, 4°C) and crypts isolated by vigorous shaking
94 in PBS. Crypt suspensions were centrifuged (fixed rotor, 88 RCF, 4°C) and the pellet washed
95 twice in cold PBS. Crypts were fixed in 4% PFA (30min, room temperature), permeabilized in
96 1% Triton-X100 (1 hour, room temperature) and blocked in Blocking Buffer (2 hours, 4°C).
97 Crypts were incubated with primary antibodies diluted in Working Buffer: Mcm2 (Cell
98 Signalling, 1:500), phospo-HistoneH3 (Abcam, 1:500), Ki67 (Abcam ab15580, 1:250), αGFP
99 (Abcam, 1:500), washed 5x with Working Buffer before overnight incubation with secondary
100 antibodies diluted in Working buffer: Alexafluor™ conjugated goat anti-mouse or anti-rabbit
101 (1:500, Molecular Probes) or stains: Rhodamine labelled Ulex Europaeus Agglutinin I (UEA,
102 1:500), 5 µg/ml Hoechst 33342 or Alexafluor™ conjugated Phalloidin (1:150), at 4°C. Crypts
103 were mounted directly on slides in Prolong Gold, overnight.

104 **CSK extraction**

105 Soluble proteins were extracted from the epithelial cells in isolated crypts by incubation
106 with CSK extraction buffer (10 mM HEPES, 100 mM NaCl, 3 mM $MgCl_2$, 1 mM EGTA, 300 mM
107 sucrose, 0.2% TritonX-100, 1 mM DTT, 2% BSA) supplemented with protease inhibitors

108 (PMSF, Pepstatin, Leupeptin, Cystatin, $Na_3VO_4$, NaF, aprotinin) for 20 minutes on ice prior to
109 fixation. Crypts were then fixed with 4% PFA and processed further.

110 **H2B-GFP label retention**

111 H2B-GFP expression in transgenic *R26-rtTA Col1A1-H2B-GFP* mice was induced by replacing
112 normal drinking water with 5% sucrose water supplemented with 2 mg/ml doxycycline.
113 After 7 days, doxycycline water was replaced with normal drinking water. Subsequently,
114 mice were sacrificed after 7 days.

115 **EdU incorporation and detection**

116 Mice were injected intraperitoneally with 100 µg EdU (Invitrogen) prepared in 200 µl sterile
117 PBS. Mice were sacrificed 1 hour or 17 hours post induction. For organoids, 10 µM EdU was
118 included in crypt media for 1 hour before harvesting. EdU was detected by Click-it
119 chemistry, by incubation in EdU working buffer (1.875 µM Alexafluor 488 azide (Invitrogen),
120 2 mM $CuSO_4$, 10 mM Ascorbic acid), overnight at 4°C, prior to processing for
121 immunofluorescence staining.

122 **Organoid Culture**

123 Isolated crypts were dissociated to single cells with TripLE express (Life Technologies) at
124 37°C, 5 minutes. Dissociated cells were filtered through a 40 µm cell strainer (Greiner) and
125 suspended in growth factor reduced Matrigel (BD Biosciences). Organoids were grown in
126 crypt media (ADF supplemented with 10 mM HEPES, 2 mM Glutamax, 1 mM N-
127 Acetylcysteine, N2 (Gemini), B27 (Life technologies), Penicillin/Streptomycin (Sigma)
128 supplemented with growth factors – ENR media (EGF (50 ng/ml, Invitrogen), Noggin (100

129 ng/ml, eBioscience) and RSpondin conditioned media produced from stably transfected L-
130 cells (1:4). Chiron99021 (3 µM), Valproic acid (1 mM, Invitrogen) and Y27632 (10 µM,
131 eBiosciences) were added to the culture for the first 48 hours. Organoids were passaged
132 every 3-5 days by mechanically disrupting Matrigel and by washing and pipetting in ADF.
133 Dissociated crypts were re-suspended in fresh Matrigel and grown in crypt media
134 supplemented with growth factors.

135 For small molecule treatments, primary intestinal epithelial cells were cultured in ENR-CVY
136 (ENR plus Chiron99021, Valproic acid and Y27632) for 3 Days, and then organoids were sub-
137 cultured in ENR for two further days prior to the start of the experiment. Organoids were
138 then treated with the stated small molecules for the indicated time periods. For induction of
139 shallow-$G_0$, organoids were treated with Gefitinib (5 µM) coupled with removal of EGF from
140 the crypt media. For re-activation, the media was removed and fresh growth factors added.
141 All growth factors and inhibitors were replenished every 2 days throughout the experiment.

142 **Flow cytometry and cell sorting**

143 Intestinal crypts were isolated and dissociated to single cells as described above. Isolated
144 cells were filtered through 40 µm cell strainers. Cells were fixed in 0.5% PFA (pH7.40, 15
145 minutes, room temperature), washed once in working buffer and permeabilized with ice-
146 cold 70% EtOH, 10 minutes. Cells were then washed in working buffer and re-suspended
147 with primary antibodies (Mcm2, 1:500; GFP, 1:500; Ki67, 1:200) diluted in Working buffer
148 (overnight, 4°C). Following two washes in working buffer, cells were re-suspended in
149 secondary antibodies goat anti-mouse or anti-rabbit (Alexafluor647, 1:500 (Molecular
150 Probes); Alexafluor488-Ki67, 1:400 (Clone SolA15, BD Biosciences), diluted in working buffer

151 (1 hour, room temperature). After two washes in working buffer, cells were suspended in
152 working buffer containing 15 µg/ml DAPI. Samples were analysed on a FACS Canto (BD
153 Biosciences) and data analysed using FlowJo (Treestar).

154 For cell sorting, cells were isolated from Lgr5-GFP mice as described above by treatment
155 with TripLE express for 15 minutes, 37ºC followed by filtration through 40 µm filters
156 (Greiner). Cells were sorted in ADF supplemented with 1% FCS and DAPI (15 µg/ml). Sorting
157 was performed using an Influx™ Cell sorter (BD biosciences). Cells were checked post-sort
158 to ensure sample purity by re-examining Lgr5 expression in the sorted gates.

159 **Microscopy and Image analysis**

160 Samples were imaged using a Zeiss LSM 710 microscope using a 40X LD Pan-Neofluar
161 objective lens and immersion oil with a refractive index of 1.514. Z-stacks were acquired at
162 optimal section intervals between 0.3 and 0.8 µm.

163 Image processing and analysis were performed using Imaris (Bitplane). Images of individual
164 crypts were manually cropped to ensure that an individual crypt was the only region of
165 interest. All nuclei were detected in individual crypts using automated thresholding in
166 Imaris, set to detect nuclei at an estimated size of 3.5 µm. Missed or incorrectly assigned
167 nuclei were manually identified. This function produced measurement points that
168 segmented the specific region at the corresponding co-ordinate of the measurement point.
169 Mean intensities for different channels were calculated per spot. This equates to the
170 intensity at the centre region of each nucleus. A reference nucleus at the crypt base was
171 used to define the crypt base position. The Euclidean distance to this point was measured
172 and defined as the distance to the crypt base. Multiple images were analysed using the

173 same workflow and the analysed files collated. For vibratome sections, a plane was
174 manually defined running through to the muscle layer beneath the epithelium. The smallest
175 distance to this surface was defined for segmented nuclei.

176

177 **RESULTS**

178 **Mcm2 expression declines along the crypt-villus axis**

179 Because of their abundance, strong conservation and association with the core DNA
180 replication process, the presence of MCM2-7 proteins is frequently used to establish
181 proliferative capacity in tissues, similar to Ki67 or PCNA (Gonzalez et al., 2005, Jurikova et
182 al., 2016, Stoeber et al., 2001, Williams et al., 1998). Usually, terminally differentiated cells
183 in mammalian tissues do not contain MCM2-7 (Stoeber et al., 2001, Todorov et al., 1998).
184 To establish the overall MCM2-7 protein abundance along intestinal crypts, we first
185 examined the expression of MCM2-7 proteins in adult murine small-intestinal epithelium
186 using high-resolution immunofluorescence microscopy. We focused on Mcm2 as a surrogate
187 for all the members of the MCM2-7 complex based on their similar function and localisation.

188 Consistent with previous reports in both murine and human intestinal epithelium, we
189 observed that Mcm2 was highly expressed in intestinal crypts (**Figure 1A**) and declined
190 gradually along the crypt-villus axis (**Figure 1B**), but persisted in a few cells in the villus
191 compartment (**S1 Figure A**). MCM2-7 are highly abundant proteins and they have a
192 relatively long (>24 hour) half-life (Musahl et al., 1998). This makes it likely that after cells
193 differentiate, their MCM2-7 content declines at a slow rate. Mcm2 was nuclear in

194 interphase cells but cytoplasmic during mitosis (**Figure 1C**). Although the majority of
195 intestinal crypt cells expressed Mcm2, at the crypt base Mcm2(+) and Mcm2(-) cells were
196 interspersed (**Figure 1A, S1 Figure A**), consistent with previous reports (Pruitt et al., 2010).
197 This pattern is reminiscent of the alternating arrangement of Lgr5(+) stem cells and Paneth
198 cells at the crypt base (Barker et al., 2007). Lgr5(+) stem cells express Ki67 and are
199 continually proliferative whereas Paneth cells are fully differentiated and are Ki67(-) (Basak
200 et al., 2014). As expected, Mcm2 was expressed in all Lgr5(+) stem cells and there was a
201 strong correlation between Mcm2 and Lgr5 expression (**Figure 1D**). This is consistent with
202 the idea that $Lgr5^{Hi}$ stem cells are the main proliferative stem cells in the intestinal crypt.
203 Staining with Ulex Europaeus Agglutinin I (UEA), demonstrated that most of the Mcm2(-)
204 cells in the crypt base were UEA(+) Paneth cells (**Figure 1E**).

205 Normally, MCM2-7 expression is lost in terminally differentiated cells (Eward et al., 2004,
206 Stoeber et al., 2001, Williams et al., 1998, Williams et al., 2004). The loss of expression has
207 been suggested as a major contributor to the proliferation-differentiated switch *in vivo.* To
208 test this idea, we measured the Mcm2 content of young and mature secretory cells in
209 intestinal crypts and villi (**Figure 1F, G**). There was differential expression of Mcm2 in distinct
210 secretory lineages. Many mature secretory cells including Paneth, Goblet and
211 enteroendocrine cells were Mcm2(-), consistent with their differentiation status and long
212 life-span in the epithelium (van der Flier and Clevers, 2009). We detected a number of
213 UEA(+) Mcm2(+) and UEA(+) Mcm2 (-) cells in intestinal crypts (**Figure 1F**). Assuming that
214 Mcm2 expression declines slowly after differentiation, Mcm2 content could reflect the
215 maturity of a particular secretory cell. Consistently, Mcm2 expression in UEA(+) cells in

216 crypts was significantly higher than in villi (**Figure 1G**), supporting the idea that Mcms are
217 gradually lost upon terminal differentiation.

218 **Visualisation of DNA replication licensing *In vivo***

219 MCM2-7 exist in three states: as hexamers free in the nucleoplasm, as double hexamers
220 bound to DNA during late mitosis, G1 and S phase, or as CMG complexes at replication forks
221 during S phase (Evrin et al., 2009, Gambus et al., 2011, Remus et al., 2009). To distinguish
222 between DNA-bound and soluble forms, we developed a protocol involving a brief
223 extraction of isolated crypts with non-ionic detergent to remove soluble MCM2-7. The
224 remaining Mcm2 should mark cells whose origins are licensed for replication. Extraction did
225 not visibly affect intestinal crypt integrity but made them more opaque compared to
226 unextracted tissue (**Figure 2A**). The majority of cells in unextracted crypts were Mcm2(+)
227 (**Figure 2B**) similar to tissue sections and mirrored the ubiquitous expression of Ki67 along
228 the crypt axis. After extraction, the majority of the Mcm2 content in cells was lost (**Figure**
229 **2B**). The labelling index of isolated crypts revealed that only 10-30% of cells were licensed
230 (**Figure 2C**). After extraction, Mcm2(+) was not present in mitotic cells expressing
231 phosphorylated histone H3, confirming the extraction procedure successfully removed non-
232 DNA bound MCM2-7 proteins (**Figure 2D**).

233 We used flow cytometry to measure MCM2-7 content more directly and further confirm the
234 effectiveness of the extraction procedure. Whereas the majority of isolated epithelial cells
235 expressed Mcm2 that persisted throughout the cell-cycle, extraction revealed a distinct
236 profile of Mcm-containing cells in crypts (**Figure 2E**) consistent with what has been reported
237 for other cells (Friedrich et al., 2005, Moreno et al., 2016). MCM2-7s are loaded onto DNA

238 throughout $G_1$, reach a maximum level before cells enter S-phase, and are subsequently
239 displaced from DNA during replication. Interestingly, we noticed that isolated Intestinal
240 epithelial cells had a large range of DNA-bound Mcm2 during $G_1$. We propose that this
241 represents intermediate stages of the transition between a fully quiescent $G_0$ state, a
242 dormant state at the $G_0/G_1$ boundary or in early $G_1$ and a population fully committed to the
243 cell-cycle, being fully licensed (**Figure 2E'**). Similar results were observed in cells isolated
244 from intestinal organoids (**Figure 2F, G**)

245 **Licensing status and cell-cycle progression along the crypt-villus axis**

246 Cell-cycle dynamics of intestinal stem and progenitor cells are highly heterogeneous (Pruitt
247 et al., 2010). The majority of Lgr5(+) stem cells are considered to be continually
248 proliferative, but with a much longer cell-cycle than transit-amplifying progenitor cells,
249 which are most commonly found in S-phase (Schepers et al., 2011). To investigate
250 proliferative fate decisions of intestinal epithelial cells, we used our MCM2-7 extraction in
251 crypts where S phase cells were labelled with the nucleoside analogue EdU. We then used
252 image analysis software to correlate Mcm2 content with cell-cycle stage along the crypt-
253 villus axis (**S1 Figure B-H**). This allowed quantification of licensing in relation to the cell-cycle
254 and 3D spatial information.

255 Figure 3A shows tissue following the MCM2-7 extraction and after a short 1 hour EdU pulse
256 to visualise S-phase. As expected, the majority of cells in the transit-amplifying
257 compartment were labelled with EdU suggesting that most cells were in S-phase, consistent
258 with early studies using BrdU and [$^3$H]-thymidine labelling (Chwalinski and Potten, 1987).
259 The patterns of replication foci were consistent with the reported S-phase replication timing

260 programme (Rhind and Gilbert, 2013). Typically, all licensed cells had intense nuclear Mcm2
261 staining. Some cells completely lacked Mcm2 and EdU labelling, suggesting they could be in
262 either $G_0$, very early $G_1$ or in $G_2$. Some cells were labelled with both Mcm2 and EdU. These
263 double-labelled cells typically showed patterns of EdU labelling consistent with early to mid
264 S phase and Mcm2 labelling of DNA compartments expected to replicate later in S phase.
265 This relationship has been observed in tissue culture cells (Krude et al., 1996) and is
266 consistent with the idea that DNA-bound MCM2-7 are displaced from chromosomal
267 domains as replication is completed. Cells with late S-phase patterns of EdU labelling had
268 little or no detectable Mcm2, consistent with the displacement of the majority of MCM2-7
269 by the end of S phase. Quantification of the nuclear intensities of Mcm2 and EdU in these
270 discrete populations (**S1 Figure H**) confirmed previous results using flow cytometry (**Figure**
271 **2E**) and allowed grouping of cells into 4 cell cycle groups: Unlicensed, $G_0/G_1$; $G_1$ licensed; S-
272 phase and Late-S/$G_2$ (**S1 Figure H**). We also measured nuclear volume, which increases
273 during S phase and $G_2$. This showed that nuclear volume increased up to two-fold in cells
274 classified as S-phase and Late-S/$G_2$ by Mcm2 and EdU staining (**Figure 3B)**. This confirms our
275 cell-cycle assignment and also suggests that most Mcm2(-) cells are in $G_0$ or $G_1$, rather than
276 in $G_2$.

277 The combination of concurrently labelling DNA-bound Mcm2 and EdU showed a clear
278 correlation between cell position and cell-cycle stage (**Figure 3C, D, E**). At the base of the
279 crypt, $G_0$/early-$G_1$ cells predominate. At increasing distances from the crypt base there is a
280 successive rise in licensed $G_1$ cells, early/mid S phase cells and then late S/$G_2$ cells. Further
281 up the crypt, at the end of the TA compartment, these cell cycle stages decline in reverse
282 order, until unlicensed $G_0$ cells again predominate. This suggests that there is a co-ordinated

283 progression through the cell division cycle as cells enter, then leave, the TA compartment.
284 This was also observed as a field effect with many neighbouring cells showing similar
285 replication patterns (**S2 Figure A, B**).

286 **Terminal differentiation is associated with a binary licensing decision**

287 At the terminal boundary of the transit-amplifying compartment, the majority of cells were
288 unlicensed and had no DNA-bound Mcm2 (**Figure 3C-E**). Similarly, there were no licensed $G_1$
289 cells beyond the TA compartment as defined by incorporation of EdU (**Figure 3F**). However,
290 total Mcm2 expression extended significantly beyond the last cells with DNA-bound Mcm2
291 or incorporated EdU (**Figure 3D, F**). The distribution of total Mcm2 expression also
292 corresponded to the zone where cells express Ki67 (**S3 Figure**). Although Mcm2 and Ki67
293 expression persists beyond the TA compartment, licensing does not occur in this area. This
294 suggests that differentiation is not governed by a gradual reduction in total MCM2-7 levels,
295 but is a binary decision and licensing is abolished immediately after the final mitosis
296 preceding differentiation. To further examine this, we marked the terminally differentiated
297 zone by a 1 hour EdU pulse, followed by a 16 hour chase (**Figure 3G, H**). After 16 hours, the
298 majority of the distal end of the TA compartment became labelled with EdU. All labelled
299 nuclei in this area were significantly smaller than EdU(+) cells at the proximal end of the TA
300 compartment (data not shown), suggestive of their differentiation status. Importantly the
301 EdU(+) differentiated cells at the distal end of the TA compartment lacked DNA-bound
302 Mcm2, supportive of the model where licensing is inhibited immediately at terminal
303 differentiation.

304 **The majority of Intestinal stem cells reside in unlicensed shallow-$G_0$' state**

305 The majority of cells in the crypt base expressed Mcm2, consistent with the finding that all
306 Lgr5(+) cells express Mcm2 but mature secretory cells, such as Paneth cells, do not (**Figure**
307 **1D, E**). Surprisingly, extraction revealed that only 7-15% of cells were licensed in the crypt
308 base (**Figure 3C, D**), with most cells in an unlicensed state despite expressing Mcm2. The
309 abundance of licensed cells peaked 40-60 µm away from the crypt base, corresponding to
310 just above the +4/+5 cell position (**Figure 3D, E**).

311 It is not possible to identify Lgr5 in these experiments, as it is extracted along with unbound
312 Mcm2. We therefore identified Paneth cells by UEA staining and considered all UEA(-) cells
313 in the crypt base to be intestinal stem cells (**Figure 4A**). >50% of the UEA(-) stem cells were
314 in an unlicensed state and were not incorporating EdU (**Figure 4B**). Approximately 30-40% of
315 all UEA(-) cells in the stem cell compartment were in an active phase of the cell cycle,
316 (**Figure 4B**) corresponding to 5-6 stem cells out of the total 14 present (Snippert et al.,
317 2010). This number is similar to the small number of proposed 'working' stem cells in the
318 crypt base (Baker et al., 2014, Kozar et al., 2013). Unlicensed cells not incorporating EdU (i.e.
319 unlabelled in this experiment) could theoretically be in either $G_0$ or in $G_2$. To distinguish
320 between these possibilities we first isolated crypt cells from Lgr5-GFP mice and measured
321 both GFP and DNA content. Both Lgr5(+) and Lgr5(-) cell populations had a similar cell-cycle
322 profile with the majority of cells having 2N DNA content (**S2 Figure C**). We also examined the
323 nuclear volume of cells at different positions along the crypt axis, after staining for EdU
324 incorporation and DNA-bound Mcm2. The majority of unlicensed cells had a similar nuclear
325 volume to fully licensed cells in $G_1$ and not cells in Late-S/$G_2$ phase (**S2 Figure D**). Together,

326 these results suggest that, although they express abundant Mcm2, the majority of intestinal
327 stem cells reside in an unlicensed state.

328 To confirm this conclusion, we flow sorted Lgr5-GFP(+) cells, extracted unbound MCM2-7
329 and stained them for Mcm2 and Ki67. Consistent with our previous results, most of the
330 Lgr5(+) cells with a 2N DNA content had low levels of DNA-bound Mcm2, and were in an
331 unlicensed state (**Figure 4Ci, ii**). Importantly, both the licensed and unlicensed cells were
332 Ki67(+) indicating that they had not withdrawn from the cell-cycle long-term (**Figure 4Cii**).

333 This state – 2N DNA content with low levels of DNA-bound Mcm2 - could be explained by
334 two, slightly different, scenarios. One possibility is that MCM2-7 are loaded on to DNA very
335 slowly in Lgr5(+) cells, thereby extending $G_1$ length (Schepers et al., 2011) (Dalton, 2015). In
336 this case, the presence of unlicensed cells simply reflects the increased time required to
337 fully license origins, and different levels of Mcm2 loading should be equally distributed
338 between $G_1$ cells. Alternatively, most Lgr5(+) cells are not in $G_1$ and do not load MCM2-7
339 until an active decision is made to enter the cell cycle and activate the licensing system, at
340 which time MCM2-7 proteins are rapidly loaded. In this case, there should be a discrete
341 peak of unlicensed cells with a $G_1$ DNA content representing cells that have withdrawn from
342 the cell cycle, and a lower frequency of $G_1$ cells that have loaded different amounts of
343 MCM2-7. To distinguish between these two possibilities, we examined the frequency
344 distribution of DNA-bound Mcm2 in Lgr5(+) cells with a 2N DNA content (**Figure 4Ciii**). The
345 distribution of DNA-bound Mcm2 cells was most similar to the predicted distribution in the
346 latter model and showed a discrete peak of unlicensed cells (**Figure 4C**). Since most of these
347 unlicensed Lgr5(+) cells express abundant Mcm2 (**Figure 1D**), they are in a state that is
348 distinct from that of previously described $G_0$ cells, which typically do not express licensing

349 proteins at all. We term this new intermediate state – where cells express abundant MCM2-
350 7 proteins that are not bound to DNA – as 'shallow-$G_0$'. Because they do not need to
351 synthesize more MCM2-7 proteins to enter the cell cycle, they are likely to be in a transient
352 state of quiescence.

353 It has previously been reported that embryonic stem cells license more replication origins
354 than neural stem/progenitor cells differentiated from them (Ge et al., 2015). To determine if
355 stem and non-stem cells in intestinal crypts behave similarly, we compared the amount of
356 DNA-bound Mcm2 in $G_1$/$G_0$ and early S phase Lgr5(+) cells with that in Lgr5(-) cells (Moreno
357 et al., 2016). Although the majority of Lgr5(+) cells were unlicensed, when they entered S
358 phase they had approximately twice as much DNA-bound Mcm2 compared to Lgr5(-) cells
359 (**Figure 4D**). This is consistent with the idea that adult intestinal stem cells license more
360 origins than TA cells. This may represent a mechanism to protect genomic integrity.

361 **Intestinal label retaining cells are in a deep $G_0$ state**

362 Although the intestinal crypt base primarily consists of Lgr5(+) stem cells there is also a
363 reserved pool of quiescent stem cells, often referred to as '+4 label retaining cells' (LRCs)
364 reflecting their position in the crypt base and their ability to retain nascent DNA labels
365 (Potten et al., 2002). These cells are a rare subset of Lgr5(+) cells which are also secretory
366 precursors (Buczacki et al., 2013). To further define the licensing status of these label-
367 retaining intestinal stem cells, we identified UEA(-) LRCs by expressing H2B-GFP (which is
368 incorporated into the chromatin of dividing cells) for 7 days and then chasing for a further 7
369 days (**S4 Figure**) (Buczacki et al., 2013, Roth et al., 2012). Labelled cells that did not divide
370 during the 7-day chase period contain high levels of H2B-GFP, and cells that divided multiple

371 times only have low levels. Strikingly, unlike the majority of the Lgr5(+) cells, quiescent LRCs
372 with high GFP-H2B did not express Mcm2 (**Figure 4E**). Consistently, only non-LRC daughter
373 cells with low levels of H2B-GFP had DNA-bound Mcm2 (**Figure 4F, G**). This shows that, as
374 expected, the LRC stem cells are in deep $G_0$, unable to license because they do not express
375 MCM2-7. In contrast, the 'active' intestinal stem cells reside in a state of shallow $G_0$,
376 expressing MCM2-7, but remain unlicensed.

377 **Stemness is associated with the unlicensed state**

378 We wished to understand how intestinal stem cells were maintained in an unlicensed state
379 and whether stemness was directly associated with the unlicensed shallow-$G_0$ state. To
380 investigate this relationship we designed a proof-of-concept assay using intestinal
381 organoids. This allowed a preliminary assessment of licensing dynamics during entry and
382 exit into quiescence. In contrast to intestinal crypts *in vivo*, intestinal organoids contained
383 considerably more cells with DNA-bound Mcm2 in their crypt-like branches (**Figure 5A**).
384 Cytometry-based quantification of cells with a 2N DNA content suggested that there were
385 approximately twice as many fully licensed cells in organoids than in intestinal crypts (**Figure**
386 **5Bi, ii**). This suggests that organoids may represent intestinal epithelium in an accelerated
387 state of self-renewal and do not fully recapitulate cell-cycle dynamics of intestinal epithelial
388 cells *in vivo*.

389 To measure licensing dynamics in organoids during entry and exit into quiescence, we
390 directly compared licensing states with the presence of Ki67. Most cells in organoids express
391 Ki67 and it increased during cell-cycle progression (**Figure 5Ci**). The DNA-bound Mcm2
392 profile was similar to that in isolated crypts (compare **Figure 5Cii** and Figure 2E). Correlating

393 Ki67 and DNA-bound Mcm2 produced a distinctive profile that is similar for isolated cells
394 from organoids and intestinal crypts. This profile reveals a population of cells that appear to
395 be losing Ki67 (dashed arrow in **Figure 5 Ciii and iv**) and which might represent cells losing
396 proliferative capacity and transitioning towards differentiation (**Figure 5C, S5 Figure A**). This
397 loss of proliferative capacity may begin in cells that express Ki67 but are unlicensed, i.e. cells
398 in shallow $G_0$. It also suggests that different stages of quiescence exist that are reflected by a
399 spectrum of Ki67 and Mcm levels. To test this idea, we induced quiescence by inhibiting the
400 EGF receptor (EGFR), which reduces MAP kinase activity and blocks DNA replication and cell
401 division (Lynch et al., 2004). Strikingly, inhibition of EGFR for 24 hours induced arrest in
402 shallow-$G_0$, and caused the majority of cells to be unlicensed with a 2N DNA content, while
403 expressing Mcm2 and Ki67 (**Figure 5Dii**). Prolonged EGFR inhibition caused a transition into
404 an intermediate state between shallow-$G_0$ and deep $G_0$, with reduced Ki67 expression but
405 with total Mcm2 levels maintained (**Figure 5Diii**). These shallow-$G_0$ states were reversible by
406 removal of EGFRi and re-addition of fresh growth factors (**Figure 5Div**).

407 We also used this assay to investigate how these shallow-$G_0$ states and stemness might be
408 related. Inhibiting EGFR also increases Lgr5 expression (Basak et al., 2017), suggesting that
409 prolonged quiescence can be associated with 'stemness'. The observed increase in shallow
410 $G_0$ cells after 24 hours EGFRi treatment is thus consistent with the idea that stem cells spend
411 time in shallow $G_0$. To test this idea more directly, we also used an alternative approach.
412 Treatment of organoids with Chir99201 (a GS3K inhibitor) and Valproic acid (a Notch
413 activator/histone deacetylase inhibitor) resulted in Lgr5 expression throughout the organoid
414 epithelium (**S5 Figure B**) (Yin et al., 2014). This treatment also caused the appearance of a
415 population of cells with low levels of Ki67 and intermediate levels of DNA-bound Mcm2

416 (**Figure 5E**) similar to the intermediate shallow $G_0$ state caused by EGFRi. Surprisingly, we
417 observed cells with low levels of Ki67 and intermediate levels of DNA-bound Mcm2,
418 suggesting that re-licensing of these cells occurs before they express high levels of Ki67.
419 Making measurements at intermediate times of CV treatment or after CV removal,
420 confirmed the existence of the intermediate and shallow $G_0$ states and also the ability to re-
421 license before Ki67 re-expression (**Figure 5F**). Combining EGFRi and CV treatment, also
422 suggested that cells can reactivated licensing from the intermediate $G_0$ state directly (**Figure**
423 **5G**).

424 Treatment with Valproic acid alone, but not Chir99021, partially recapitulated this effect,
425 suggesting that active Notch signalling is involved (**S5 Figure C**). Inhibiting Notch signalling
426 with DAPT treatment, which induces terminal secretory cell differentiation (van Es et al.,
427 2005), caused an induction of deep-$G_0$, with reduced Ki67 and a loss of Mcm2 proteins (**S5**
428 **Figure D**). Together, this suggests that Notch signalling can affect the transition between
429 deep and shallow-$G_0$ states.

430 **Discussion**

431 The cell-cycle of intestinal stem and transit-amplifying cells is poorly understood. By
432 comparing the total and DNA-bound Mcm2 in intact intestinal crypts we provide new
433 insights into how licensing and cell-cycle commitment are coupled in this tissue. We provide
434 evidence that after their final mitosis, transit amplifying cells do not license their replication
435 origins and so immediately exit the cell cycle. We show that normally the majority of Lgr5(+)
436 stem cells reside in an unlicensed state, despite expressing Mcm2 and Ki67. In this state of
437 shallow-$G_0$, stem cells might be poised to easily re-enter the cell division cycle.

438 Lgr5(+) stem cells have a cell-cycle length greater than transit-amplifying cells (Schepers et
439 al., 2011). The biological relevance of this is currently unknown. The data presented here
440 suggest a delay in origin licensing is responsible for the prolonged cell-cycle of Lgr5(+) cells.
441 Although ~80% of Lgr5(+) cells are thought to be continually proliferative and express high
442 levels of both Ki67 (Basak et al., 2014) and Mcm2, we found that most Lgr5(+) cells reside in
443 an unlicensed state, with 2N DNA content and Mcm2 not bound to DNA. Since the licensed
444 state defines proliferative fate commitment, we suggest that these cells are in a prolonged
445 state of shallow quiescence, which we term shallow $G_0$, expressing proliferative makers such
446 as Ki67 and Mcm2 without committing to proliferation since Mcm2 is not bound to DNA
447 (**Figure 6**). The number of Lgr5(+) cells with DNA bound-Mcm2 was similar to the number of
448 proposed 'active' stem cells determined in lineage tracing experiments (Baker et al., 2014,
449 Kozar et al., 2013).

450 Prolonged arrest may eventually result in degradation of MCM2-7 proteins and lead to
451 induction of a state of deep quiescence. Consistent with this idea, we observed that LRCs,
452 thought to provide a reserve of quiescent stem cells, did not express Mcm2. The lack of
453 Mcm2 expression may reflect that a significant period of time has passed since these cells
454 divided. The delay in activating the licensing system may create a prolonged time-window
455 for Lgr5(+) cells to receive and interpret environmental cues before deciding to commit to
456 duplication, offering a means to control their number. It is likely that the majority of Lgr5(+)
457 cells eventually re-enter the cell cycle, given their continual expression of proliferation
458 markers (Basak et al., 2014). The identity and decisions of Lgr5(+) cells are likely governed by
459 stochastic choices and the ability to enter a shallow $G_0$ stage offers unique flexibility for
460 stem cells to make these choices. Consistent with this idea, modulation of the stem cell

niche by Chir99021 and Valproic acid induces stemness throughout the crypt-villus axis (Yin et al., 2014) and also significantly enriches a unique population of unlicensed cells with unique cell-cycle dynamics. The increase in Lgr5(+) cells in response to Valproic acid and Chir99021 suggests a corresponding increase in the number of Lgr5(+) reserve stem cells, which are in deep $G_0$ (Buczacki et al., 2013). We propose that the reactivation of these cells by injury for instance, could proceed via the intermediate $G_0$ state we describe. Initially, these cells must re-express Mcm proteins and then can directly commit to the cell-cycle from the intermediat-$G_0$ state (**S5 Figure E**). Together, this demonstrates the unique cell-cycle characteristics of intestinal stem cells, which can be functionally defined by the licensed state.

Growing evidence suggests that intestinal stem cell fate is not governed by asymmetric segregation of fate determinants (Lopez-Garcia et al., 2010, Snippert et al., 2010, Steinhauser et al., 2012). Components of the stem cell niche, such as the combination of Wnt and Notch signalling can affect stem cell fate decisions and also reduce the cycle rate of intestinal stem cells (Hirata et al., 2013). This is consistent with the idea that as well as decreasing proliferation rate, increased $G_0/G_1$ length might underpin cell fate choices. Indeed, $G_1$ elongation of mouse and human embryonic stem cells can drive differentiation (Calder et al., 2013, Coronado et al., 2013). Similarly, long $G_1$ phases are associated with the production of fate-restricted progenitors during neurogenesis (Arai et al., 2011). This has been suggested to be facilitated by an extended time window in the cell-cycle to allow niche factors and/or fate determinants to (Calegari and Huttner, 2003). In the case of intestinal stem cells, holding cells in shallow $G_0$ may allow an extended time for stem cell fate factors to act and maintain stem cell fate.

**Delayed activation of the DNA replication licensing system in Lgr5(+) intestinal stem cells**

484 Like embryonic stem cells (Ge et al., 2015), intestinal stem cells appear to have licensed
485 more origins than non-stem cells when they enter S phase. Intestinal stem cells may
486 therefore more readily engage the licensing checkpoint that ensures that all origins are
487 licensed before cells enter S phase (Alver et al., 2014, Liu et al., 2009, Shreeram et al., 2002).
488 This additional demand for licensed origins in stem cells may explain why crypts
489 hypomorphic for Mcm2 have a stem-cell deficiency (Pruitt et al., 2007).

490 Terminal differentiation in the intestinal epithelium is associated with disengagement from
491 the proliferative niche and involves the gradual dilution of niche factors, which causes cells
492 to exit the cell-cycle (Farin et al., 2016, Mariadason et al., 2005). Consistent with previous
493 reports, we observed that Mcm2 expression gradually declined along the crypt-villus axis
494 (**Figure 1**) (Stoeber et al., 2001). We also found that there is an abrupt loss of DNA-bound
495 Mcm2 as cells exit the transit amplifying zone and undergo terminal differentiation. This
496 suggests that the proliferation-differentiation switch is a binary decision made in the last cell
497 cycle in the mid-upper transit-amplifying compartment.

498 It is unclear why licensing is rapidly inhibited at the top of the transit amplifying zone or in
499 most of the Lgr5(+) stem cells. The simplest explanation is that licensing factors such as Cdt1
500 or Cdc6 are not readily available in new-born stem cells, and their synthesis has to be
501 directed by an upstream signal for fate commitment. This occurs after prolonged quiescence
502 which is accompanied by passive downregulation of such licensing factors (Coller, 2007). In
503 contrast, in continually dividing cells their levels are maintained. Consistently, licensing
504 factors such as Cdc6, along with many cyclin-CDK complexes, are down regulated beyond
505 the end of the TA zone (Frey et al., 2000) (Smartt et al., 2007).

506 In summary, we demonstrate that the dynamics of the DNA replication licensing system
507 provides a new way of measuring the proliferative fate of intestinal stem cells. We suggest a
508 model for 'working' intestinal stem cells that reside in a state of shallow quiescence until a
509 proliferative fate decision is made. Consistent exit from the cell-cycle in label retaining '+4'
510 cells leads to loss of proliferative capacity and loss of Mcm2 expression causing cells to enter
511 a deeply quiescent state (**Figure 6**). We suggest that the shallow-$G_0$ state serves stem cells in
512 controlling their numbers by regulating the cell-cycle.

513 **Author contributions**

514 T.D.C, J.J.B and I.N conceived and designed the study; T.D.C collected the data and
515 performed the analysis; I.P.N assisted with animal experiments; T.D.C wrote the manuscript
516 with assistance from I.N and J.J.B.

517 **Conflicts of Interest**

518 The authors report no conflicts of interest.

519 **Acknowledgements**

520 We would like to thank members of the Näthke and Blow laboratories for general assistance
521 and helpful discussions. We thank Dr Paul Appleton, Dr Graeme Ball and the Dundee
522 Imaging and Tissue Imaging Facility for support with microscopy and image analysis. The
523 imaging facility is funded by the Welcome Trust Technology Platform award
524 (097945/B/11/Z) and Welcome Trust award (101468/Z/13/Z). We thank Dr Rosemary Clarke
525 and the Dundee Flow Cytometry Facility for support with flow cytometry, cell sorting and
526 analysis. This work was supported by a programme grant from Cancer Research UK to I.N

(C430/A11243) and to J.J.B (C303/A14301), Wellcome Trust grant WT096598MA and an MRC studentship award to T.D.C.

## REFERENCES

ALVER, R. C., CHADHA, G. S. & BLOW, J. J. 2014. The contribution of dormant origins to genome stability: from cell biology to human genetics. *DNA repair,* 19**,** 182-9.

ARAI, Y., PULVERS, J. N., HAFFNER, C., SCHILLING, B., NUSSLEIN, I., CALEGARI, F. & HUTTNER, W. B. 2011. Neural stem and progenitor cells shorten S-phase on commitment to neuron production. *Nature communications,* 2**,** 154.

BAKER, A. M., CERESER, B., MELTON, S., FLETCHER, A. G., RODRIGUEZ-JUSTO, M., TADROUS, P. J., HUMPHRIES, A., ELIA, G., MCDONALD, S. A., WRIGHT, N. A., SIMONS, B. D., JANSEN, M. & GRAHAM, T. A. 2014. Quantification of crypt and stem cell evolution in the normal and neoplastic human colon. *Cell reports,* 8**,** 940-7.

BARKER, N., VAN ES, J. H., KUIPERS, J., KUJALA, P., VAN DEN BORN, M., COZIJNSEN, M., HAEGEBARTH, A., KORVING, J., BEGTHEL, H., PETERS, P. J. & CLEVERS, H. 2007. Identification of stem cells in small intestine and colon by marker gene Lgr5. *Nature,* 449**,** 1003-7.

BASAK, O., BEUMER, J., WIEBRANDS, K., SENO, H., VAN OUDENAARDEN, A. & CLEVERS, H. 2017. Induced Quiescence of Lgr5+ Stem Cells in Intestinal Organoids Enables Differentiation of Hormone-Producing Enteroendocrine Cells. *Cell stem cell,* 20**,** 177-190 e4.

BASAK, O., VAN DE BORN, M., KORVING, J., BEUMER, J., VAN DER ELST, S., VAN ES, J. H. & CLEVERS, H. 2014. Mapping early fate determination in Lgr5+ crypt stem cells using a novel Ki67-RFP allele. *The EMBO journal,* 33**,** 2057-68.

BLOW, J. J. & HODGSON, B. 2002. Replication licensing--defining the proliferative state? *Trends in cell biology,* 12**,** 72-8.

BUCZACKI, S. J., ZECCHINI, H. I., NICHOLSON, A. M., RUSSELL, R., VERMEULEN, L., KEMP, R. & WINTON, D. J. 2013. Intestinal label-retaining cells are secretory precursors expressing Lgr5. *Nature,* 495**,** 65-9.

CALDER, A., ROTH-ALBIN, I., BHATIA, S., PILQUIL, C., LEE, J. H., BHATIA, M., LEVADOUX-MARTIN, M., MCNICOL, J., RUSSELL, J., COLLINS, T. & DRAPER, J. S. 2013. Lengthened G1 phase indicates differentiation status in human embryonic stem cells. *Stem cells and development,* 22**,** 279-95.

CALEGARI, F. & HUTTNER, W. B. 2003. An inhibition of cyclin-dependent kinases that lengthens, but does not arrest, neuroepithelial cell cycle induces premature neurogenesis. *Journal of cell science,* 116**,** 4947-55.

CHAMPERIS TSANIRAS, S., KANELLAKIS, N., SYMEONIDOU, I. E., NIKOLOPOULOU, P., LYGEROU, Z. & TARAVIRAS, S. 2014. Licensing of DNA replication, cancer, pluripotency and differentiation: an interlinked world? *Seminars in cell & developmental biology,* 30**,** 174-80.

567 CHWALINSKI, S. & POTTEN, C. S. 1987. Influence of irradiation or thymidine (TdR) on the
568 pattern of 3H-TdR incorporation at each cell position in the crypts of the small
569 intestine of the mouse. *International journal of radiation biology and related studies*
570 *in physics, chemistry, and medicine,* 51**,** 243-54.
571 COLLER, H. A. 2007. What's taking so long? S-phase entry from quiescence versus
572 proliferation. *Nature reviews. Molecular cell biology,* 8**,** 667-70.
573 CORONADO, D., GODET, M., BOURILLOT, P. Y., TAPPONNIER, Y., BERNAT, A., PETIT, M.,
574 AFANASSIEFF, M., MARKOSSIAN, S., MALASHICHEVA, A., IACONE, R., ANASTASSIADIS,
575 K. & SAVATIER, P. 2013. A short G1 phase is an intrinsic determinant of naive
576 embryonic stem cell pluripotency. *Stem cell research,* 10**,** 118-31.
577 DALTON, S. 2015. Linking the Cell Cycle to Cell Fate Decisions. *Trends in cell biology,* 25**,** 592-
578 600.
579 DIMITROVA, D. S., PROKHOROVA, T. A., BLOW, J. J., TODOROV, I. T. & GILBERT, D. M. 2002.
580 Mammalian nuclei become licensed for DNA replication during late telophase.
581 *Journal of cell science,* 115**,** 51-9.
582 EVRIN, C., CLARKE, P., ZECH, J., LURZ, R., SUN, J., UHLE, S., LI, H., STILLMAN, B. & SPECK, C.
583 2009. A double-hexameric MCM2-7 complex is loaded onto origin DNA during
584 licensing of eukaryotic DNA replication. *Proceedings of the National Academy of*
585 *Sciences of the United States of America,* 106**,** 20240-5.
586 EWARD, K. L., OBERMANN, E. C., SHREERAM, S., LODDO, M., FANSHAWE, T., WILLIAMS, C.,
587 JUNG, H. I., PREVOST, A. T., BLOW, J. J., STOEBER, K. & WILLIAMS, G. H. 2004. DNA
588 replication licensing in somatic and germ cells. *Journal of cell science,* 117**,** 5875-86.
589 FARIN, H. F., JORDENS, I., MOSA, M. H., BASAK, O., KORVING, J., TAURIELLO, D. V., DE
590 PUNDER, K., ANGERS, S., PETERS, P. J., MAURICE, M. M. & CLEVERS, H. 2016.
591 Visualization of a short-range Wnt gradient in the intestinal stem-cell niche. *Nature,*
592 530**,** 340-3.
593 FREY, M. R., CLARK, J. A., LEONTIEVA, O., URONIS, J. M., BLACK, A. R. & BLACK, J. D. 2000.
594 Protein kinase C signaling mediates a program of cell cycle withdrawal in the
595 intestinal epithelium. *The Journal of cell biology,* 151**,** 763-78.
596 FRIEDRICH, T. D., BEDNER, E., DARZYNKIEWICZ, Z. & LEHMAN, J. M. 2005. Distinct patterns
597 of MCM protein binding in nuclei of S phase and rereplicating SV40-infected monkey
598 kidney cells. *Cytometry. Part A : the journal of the International Society for Analytical*
599 *Cytology,* 68**,** 10-8.
600 GAMBUS, A., KHOUDOLI, G. A., JONES, R. C. & BLOW, J. J. 2011. MCM2-7 form double
601 hexamers at licensed origins in Xenopus egg extract. *The Journal of biological*
602 *chemistry,* 286**,** 11855-64.
603 GE, X. Q., HAN, J., CHENG, E. C., YAMAGUCHI, S., SHIMA, N., THOMAS, J. L. & LIN, H. 2015.
604 Embryonic Stem Cells License a High Level of Dormant Origins to Protect the
605 Genome against Replication Stress. *Stem cell reports,* 5**,** 185-94.
606 GONZALEZ, M. A., TACHIBANA, K. E., LASKEY, R. A. & COLEMAN, N. 2005. Control of DNA
607 replication and its potential clinical exploitation. *Nature reviews. Cancer,* 5**,** 135-41.
608 HALAND, T. W., BOYE, E., STOKKE, T., GRALLERT, B. & SYLJUASEN, R. G. 2015. Simultaneous
609 measurement of passage through the restriction point and MCM loading in single
610 cells. *Nucleic acids research,* 43**,** e150.
611 HIRATA, A., UTIKAL, J., YAMASHITA, S., AOKI, H., WATANABE, A., YAMAMOTO, T., OKANO,
612 H., BARDEESY, N., KUNISADA, T., USHIJIMA, T., HARA, A., JAENISCH, R.,

613 HOCHEDLINGER, K. & YAMADA, Y. 2013. Dose-dependent roles for canonical Wnt
614 signalling in de novo crypt formation and cell cycle properties of the colonic
615 epithelium. *Development,* 140**,** 66-75.
616 ILVES, I., PETOJEVIC, T., PESAVENTO, J. J. & BOTCHAN, M. R. 2010. Activation of the MCM2-7
617 helicase by association with Cdc45 and GINS proteins. *Molecular cell,* 37**,** 247-58.
618 JURIKOVA, M., DANIHEL, L., POLAK, S. & VARGA, I. 2016. Ki67, PCNA, and MCM proteins:
619 Markers of proliferation in the diagnosis of breast cancer. *Acta histochemica,* 118**,**
620 544-52.
621 KINGSBURY, S. R., LODDO, M., FANSHAWE, T., OBERMANN, E. C., PREVOST, A. T., STOEBER,
622 K. & WILLIAMS, G. H. 2005. Repression of DNA replication licensing in quiescence is
623 independent of geminin and may define the cell cycle state of progenitor cells.
624 *Experimental cell research,* 309**,** 56-67.
625 KOZAR, S., MORRISSEY, E., NICHOLSON, A. M., VAN DER HEIJDEN, M., ZECCHINI, H. I., KEMP,
626 R., TAVARE, S., VERMEULEN, L. & WINTON, D. J. 2013. Continuous clonal labeling
627 reveals small numbers of functional stem cells in intestinal crypts and adenomas. *Cell*
628 *stem cell,* 13**,** 626-33.
629 KRUDE, T., MUSAHL, C., LASKEY, R. A. & KNIPPERS, R. 1996. Human replication proteins
630 hCdc21, hCdc46 and P1Mcm3 bind chromatin uniformly before S-phase and are
631 displaced locally during DNA replication. *Journal of cell science,* 109 ( Pt 2)**,** 309-18.
632 LEONE, G., DEGREGORI, J., YAN, Z., JAKOI, L., ISHIDA, S., WILLIAMS, R. S. & NEVINS, J. R.
633 1998. E2F3 activity is regulated during the cell cycle and is required for the induction
634 of S phase. *Genes & development,* 12**,** 2120-30.
635 LIU, P., SLATER, D. M., LENBURG, M., NEVIS, K., COOK, J. G. & VAZIRI, C. 2009. Replication
636 licensing promotes cyclin D1 expression and G1 progression in untransformed
637 human cells. *Cell cycle,* 8**,** 125-36.
638 LOPEZ-GARCIA, C., KLEIN, A. M., SIMONS, B. D. & WINTON, D. J. 2010. Intestinal stem cell
639 replacement follows a pattern of neutral drift. *Science,* 330**,** 822-5.
640 LYNCH, T. J., BELL, D. W., SORDELLA, R., GURUBHAGAVATULA, S., OKIMOTO, R. A.,
641 BRANNIGAN, B. W., HARRIS, P. L., HASERLAT, S. M., SUPKO, J. G., HALUSKA, F. G.,
642 LOUIS, D. N., CHRISTIANI, D. C., SETTLEMAN, J. & HABER, D. A. 2004. Activating
643 mutations in the epidermal growth factor receptor underlying responsiveness of
644 non-small-cell lung cancer to gefitinib. *The New England journal of medicine,* 350**,**
645 2129-39.
646 MAKAROVA, K. S., KOONIN, E. V. & KELMAN, Z. 2012. The CMG (CDC45/RecJ, MCM, GINS)
647 complex is a conserved component of the DNA replication system in all archaea and
648 eukaryotes. *Biology direct,* 7**,** 7.
649 MARIADASON, J. M., NICHOLAS, C., L'ITALIEN, K. E., ZHUANG, M., SMARTT, H. J., HEERDT, B.
650 G., YANG, W., CORNER, G. A., WILSON, A. J., KLAMPFER, L., ARANGO, D. &
651 AUGENLICHT, L. H. 2005. Gene expression profiling of intestinal epithelial cell
652 maturation along the crypt-villus axis. *Gastroenterology,* 128**,** 1081-8.
653 MORENO, A., CARRINGTON, J. T., ALBERGANTE, L., AL MAMUN, M., HAAGENSEN, E. J.,
654 KOMSELI, E. S., GORGOULIS, V. G., NEWMAN, T. J. & BLOW, J. J. 2016. Unreplicated
655 DNA remaining from unperturbed S phases passes through mitosis for resolution in
656 daughter cells. *Proceedings of the National Academy of Sciences of the United States*
657 *of America,* 113**,** E5757-64.

658 MOYER, S. E., LEWIS, P. W. & BOTCHAN, M. R. 2006. Isolation of the Cdc45/Mcm2-7/GINS
659 (CMG) complex, a candidate for the eukaryotic DNA replication fork helicase.
660 *Proceedings of the National Academy of Sciences of the United States of America,*
661 103**,** 10236-41.
662 MUNOZ, J., STANGE, D. E., SCHEPERS, A. G., VAN DE WETERING, M., KOO, B. K., ITZKOVITZ,
663 S., VOLCKMANN, R., KUNG, K. S., KOSTER, J., RADULESCU, S., MYANT, K., VERSTEEG,
664 R., SANSOM, O. J., VAN ES, J. H., BARKER, N., VAN OUDENAARDEN, A., MOHAMMED,
665 S., HECK, A. J. & CLEVERS, H. 2012. The Lgr5 intestinal stem cell signature: robust
666 expression of proposed quiescent '+4' cell markers. *The EMBO journal,* 31**,** 3079-91.
667 MUSAHL, C., HOLTHOFF, H. P., LESCH, R. & KNIPPERS, R. 1998. Stability of the replicative
668 Mcm3 protein in proliferating and differentiating human cells. *Experimental cell*
669 *research,* 241**,** 260-4.
670 NAMDAR, M. & KEARSEY, S. E. 2006. Analysis of Mcm2-7 chromatin binding during anaphase
671 and in the transition to quiescence in fission yeast. *Experimental cell research,* 312**,**
672 3360-9.
673 OHTANI, K., IWANAGA, R., NAKAMURA, M., IKEDA, M., YABUTA, N., TSURUGA, H. & NOJIMA,
674 H. 1999. Cell growth-regulated expression of mammalian MCM5 and MCM6 genes
675 mediated by the transcription factor E2F. *Oncogene,* 18**,** 2299-309.
676 POTTEN, C. S. & LOEFFLER, M. 1990. Stem cells: attributes, cycles, spirals, pitfalls and
677 uncertainties. Lessons for and from the crypt. *Development,* 110**,** 1001-20.
678 POTTEN, C. S., OWEN, G. & BOOTH, D. 2002. Intestinal stem cells protect their genome by
679 selective segregation of template DNA strands. *Journal of cell science,* 115**,** 2381-8.
680 PRUITT, S. C., BAILEY, K. J. & FREELAND, A. 2007. Reduced Mcm2 expression results in severe
681 stem/progenitor cell deficiency and cancer. *Stem cells,* 25**,** 3121-32.
682 PRUITT, S. C., FREELAND, A. & KUDLA, A. 2010. Cell cycle heterogeneity in the small
683 intestinal crypt and maintenance of genome integrity. *Stem cells,* 28**,** 1250-9.
684 REMUS, D., BEURON, F., TOLUN, G., GRIFFITH, J. D., MORRIS, E. P. & DIFFLEY, J. F. 2009.
685 Concerted loading of Mcm2-7 double hexamers around DNA during DNA replication
686 origin licensing. *Cell,* 139**,** 719-30.
687 RHIND, N. & GILBERT, D. M. 2013. DNA replication timing. *Cold Spring Harbor perspectives in*
688 *biology,* 5**,** a010132.
689 ROTH, S., FRANKEN, P., SACCHETTI, A., KREMER, A., ANDERSON, K., SANSOM, O. & FODDE,
690 R. 2012. Paneth cells in intestinal homeostasis and tissue injury. *PloS one,* 7**,** e38965.
691 SCHEPERS, A. G., VRIES, R., VAN DEN BORN, M., VAN DE WETERING, M. & CLEVERS, H. 2011.
692 Lgr5 intestinal stem cells have high telomerase activity and randomly segregate their
693 chromosomes. *The EMBO journal,* 30**,** 1104-9.
694 SHREERAM, S., SPARKS, A., LANE, D. P. & BLOW, J. J. 2002. Cell type-specific responses of
695 human cells to inhibition of replication licensing. *Oncogene,* 21**,** 6624-32.
696 SMARTT, H. J., GUILMEAU, S., NASSER, S. V., NICHOLAS, C., BANCROFT, L., SIMPSON, S. A.,
697 YEH, N., YANG, W., MARIADASON, J. M., KOFF, A. & AUGENLICHT, L. H. 2007. p27kip1
698 Regulates cdk2 activity in the proliferating zone of the mouse intestinal epithelium:
699 potential role in neoplasia. *Gastroenterology,* 133**,** 232-43.
700 SNIPPERT, H. J., VAN DER FLIER, L. G., SATO, T., VAN ES, J. H., VAN DEN BORN, M., KROON-
701 VEENBOER, C., BARKER, N., KLEIN, A. M., VAN RHEENEN, J., SIMONS, B. D. &
702 CLEVERS, H. 2010. Intestinal crypt homeostasis results from neutral competition
703 between symmetrically dividing Lgr5 stem cells. *Cell,* 143**,** 134-44.

704 STEINHAUSER, M. L., BAILEY, A. P., SENYO, S. E., GUILLERMIER, C., PERLSTEIN, T. S., GOULD,
705 A. P., LEE, R. T. & LECHENE, C. P. 2012. Multi-isotope imaging mass spectrometry
706 quantifies stem cell division and metabolism. *Nature,* 481**,** 516-9.
707 STOEBER, K., TLSTY, T. D., HAPPERFIELD, L., THOMAS, G. A., ROMANOV, S., BOBROW, L.,
708 WILLIAMS, E. D. & WILLIAMS, G. H. 2001. DNA replication licensing and human cell
709 proliferation. *Journal of cell science,* 114**,** 2027-41.
710 SYMEONIDOU, I. E., KOTSANTIS, P., ROUKOS, V., RAPSOMANIKI, M. A., GRECCO, H. E.,
711 BASTIAENS, P., TARAVIRAS, S. & LYGEROU, Z. 2013. Multi-step loading of human
712 minichromosome maintenance proteins in live human cells. *The Journal of biological*
713 *chemistry,* 288**,** 35852-67.
714 TODOROV, I. T., WERNESS, B. A., WANG, H. Q., BUDDHARAJU, L. N., TODOROVA, P. D.,
715 SLOCUM, H. K., BROOKS, J. S. & HUBERMAN, J. A. 1998. HsMCM2/BM28: a novel
716 proliferation marker for human tumors and normal tissues. *Laboratory investigation;*
717 *a journal of technical methods and pathology,* 78**,** 73-8.
718 VAN DER FLIER, L. G. & CLEVERS, H. 2009. Stem cells, self-renewal, and differentiation in the
719 intestinal epithelium. *Annual review of physiology,* 71**,** 241-60.
720 VAN ES, J. H., VAN GIJN, M. E., RICCIO, O., VAN DEN BORN, M., VOOIJS, M., BEGTHEL, H.,
721 COZIJNSEN, M., ROBINE, S., WINTON, D. J., RADTKE, F. & CLEVERS, H. 2005.
722 Notch/gamma-secretase inhibition turns proliferative cells in intestinal crypts and
723 adenomas into goblet cells. *Nature,* 435**,** 959-63.
724 WILLIAMS, G. H., ROMANOWSKI, P., MORRIS, L., MADINE, M., MILLS, A. D., STOEBER, K.,
725 MARR, J., LASKEY, R. A. & COLEMAN, N. 1998. Improved cervical smear assessment
726 using antibodies against proteins that regulate DNA replication. *Proceedings of the*
727 *National Academy of Sciences of the United States of America,* 95**,** 14932-7.
728 WILLIAMS, G. H., SWINN, R., PREVOST, A. T., DE CLIVE-LOWE, P., HALSALL, I., GOING, J. J.,
729 HALES, C. N., STOEBER, K. & MIDDLETON, S. J. 2004. Diagnosis of oesophageal cancer
730 by detection of minichromosome maintenance 5 protein in gastric aspirates. *British*
731 *journal of cancer,* 91**,** 714-9.
732 YIN, X., FARIN, H. F., VAN ES, J. H., CLEVERS, H., LANGER, R. & KARP, J. M. 2014. Niche-
733 independent high-purity cultures of Lgr5+ intestinal stem cells and their progeny.
734 *Nature methods,* 11**,** 106-12.

735

736

737

738 **Figure Legends**

739 **Figure 1. Mcm2 is expressed ubiquitously along the crypt-villus axis and declines slowly as**
740 **cells differentiate**

741 (**A**) Sections of normal human (top panel) and mouse (bottom panel) small-intestine were
742 stained with Phalloidin (Green) and an antibody against Mcm2 (Red). Scale bars: 200 µm.

743 (**B**) Mean Mcm2 intensities for segmented nuclei were plotted along the crypt-villus axis for
744 mouse and human tissue. Location of the crypt and villus domains is indicated.

745 (**C**) An intestinal crypt stained with Hoechst (Blue), Phalloidin (Green) and an antibody
746 against Mcm2 (Red). Individual cells in interphase and mitosis (metaphase and cytokinesis)
747 are outlined by dashed white lines.
748
749 (**D**) Images of Lgr5-GFP stem cells (Green) (top panel) co-stained with a Mcm2 antibody
750 (Red). The correlation (Pearson's correlation R=0.81, p<0.0001) between mean Mcm2 and
751 Lgr5-GFP intensities for 69 Lgr5-GFP(+) cells normalised to the maximum intensity for an
752 individual crypt is shown.

753 (**E**) Images of UEA(+) Paneth Cells (top panels) co-stained with an Mcm2 antibody (Red) and
754 UEA (Green). Mean Mcm2 intensity for segmented nuclei of UEA(+) Paneth cells was
755 compared with interphase cells (Right panels).

756 (**F**) Mcm2 (Green) and UEA (Red) expression in subsets of UEA(+) cells in crypt and villus
757 domains. UEA(+) cells at the crypt base represent Paneth cells.

758 (**G**) Quantification of mean Mcm2 intensity in individual UEA(+) cell populations. UEA(+) cells
759 in the crypt base (Paneth cells, N=224), in the upper crypt compartment (Crypt, N = 132) and
760 in the villus compartment (Villus, N = 225) were identified manually, and the nuclear Mcm2
761 intensity was determined for individual cells (All cells, N = 33,736). There was a significant
762 difference between UEA(+) cells in the crypt and villus compartments (T test, p<0.0001)

763

764 **Figure 2. Visualising Mcm2 licensing in intestinal crypts**

765 (**A**) Representative bright-field images of extracted and unextracted isolated intestinal
766 crypts. Scale bar: 90 µm

767 (**B**) Representative images of isolated crypts stained with antibodies against Mcm2 (Red) or
768 Ki67 (Purple). Scale bar: 10 µm

769 (**C**) The Mcm2 labelling index for unextracted and extracted crypts is significantly different
770 (Mean +/- SEM, N=10 crypts (T test, $p<0.0001$).

771 (**D**) Representative intestinal crypts stained with Hoechst (Blue) and antibodies against
772 Mcm2 (Red) and phospho-histone H3 (pH-H3) (Green).

773 (**E**) Representative flow cytometry profiles for extracted and unextracted isolated crypt
774 epithelial cells showing Mcm2 vs. DNA content.

775 (**E'**) Suggested model of the licensing profile shown in panel E. Deeply quiescent cells, do not
776 express Mcm2 and have a very low Mcm2 signal. Cells expressing only soluble Mcm2 ($G_0$/
777 $G_1$) show a similar Mcm2 signal to $G_2$ cells. After a proliferative fate decision has been made,
778 cells license and become committed to S-phase entry. Cells enter S-phase after maximal
779 origin licensing (Active-$G_1$). During S-phase, Mcms are then displaced from DNA during
780 replication.

781 (**F**) Representative images of extracted and unextracted intestinal organoids stained with an
782 antibody against Mcm2 (Red).

783 (**G**) The Mcm2 labelling index for unextracted and extracted organoids. Data is displayed as
784 Mean +/- SEM, N = 3 organoids and shows a significant difference (T test, $p<0.0001$).

**Figure 3. The licensing state defines distinct proliferative zones in intestinal crypts**

(**A**) Representative image of an extracted intestinal crypt isolated after a 1 hour EdU pulse *in vivo* (EdU, Green) and stained with Hoechst (Blue) and antibodies against Mcm2 (Red) and pH-H3 (White). Co-staining shows distinct cell-cycle phases (bottom panels): Licensed cells committed in $G_1$ (Mcm2(+), EdU(-)); Early (Mcm2(+), EdU(+)) to Late (Mcm2(-), EdU(+)) S-phase), and mitotic cells (pH-H3(+)). Negative cells represent deeply quiescent ($G_0$), terminally differentiated cells or cells in $G_1$, which have not made a proliferative fate decision, remaining unlicensed. The crypt base is to the left of the displayed image.

(**B**) Nuclear volume was estimated in cells at the distinct cell-cycle phases identified previously: Negative ($G_0$/$G_1$/$G_2$: N =115), $G_1$ Licensed (Mcm(+), EdU(-): N=38), S-phase (Mcm(+), EdU(+): N=24) and Late-S/$G_2$ (Mcm(-), EdU(+): N=26). Top Panels show representative examples of each cell-cycle phase and the associated 3D rendered nuclei. There was a significant difference in the size of Licensed $G_1$, S and Late-S/$G_2$ nuclei (T test, $p<0.0001$).

(**C**) Representative images of intestinal crypts isolated after a 1 hour EdU pulse (Green) *in vivo*. Displayed are 3D projections of extracted and unextracted crypts stained with Hoechst (Blue) and an antibody against Mcm2 (Red).

(**D**) Comparison between cells expressing Mcm2 protein and DNA-bound Mcm2 along the crypt-villus axis between unextracted (N=101 crypts) and extracted (N=109 crypts) (taken from 3 mice). Data is displayed as the mean % of cells per set distance bin.

(**E**) All cells were divided into 4 distinct groups based on Mcm2 and EdU intensities. These groups represent distinctive cell-cycle phases as defined by their total (unextracted N=101 crypts) or licensed (extracted N=109 crypts) Mcm2 content: **Extracted:** 1) **Unlicensed** (Mcm2(-), EdU(-)), 2) **$G_1$ licensed** (Mcm2(+), EdU(-)), 3) **Early/Mid S-phase** (Mcm2(+), EdU(+)) and 4) **Late-S/$G_2$** (Mcm2(-), EdU (+)). The data is represented as the population mean of the total cells per distance bin, Mean +/- SEM.
(**F**) The distance of the most distal Mcm2(+) and EdU(+) cells to the crypt base was compared in extracted and unextracted crypts. Data was scored manually for 10 representative crypts per condition. Licensed cells (Mcm2(+)) were significantly closer to the crypt base than EdU(+) cells (T test, $p=0.0015$. Cells expressing Mcm2 protein extended significantly above the last EdU(+) cell (T test, $p<0.0003$)

(**G**) Representative images of crypts isolated 17 hours after administration of EdU (Green). 3D projections of extracted and unextracted crypts stained with Hoechst (Blue) and an antibody against Mcm2 (Red) are shown.

(**H**) Cells were divided into 4 distinct groups as in Panel **E** (N=51 Crypts).

823 **Figure 4. Intestinal stem cells reside in an unlicensed shallow' $G_0$**

824 (**A**) Representative image of an extracted crypt base isolated 1 hour after a pulse of EdU
825 (Green) and stained with Hoechst (Blue), UEA (Red) and antibodies against Mcm2 (White).
826 Nuclear morphology and UEA signal were used to distinguish between UEA(+) Paneth Cells
827 (Dashed outline, blue stars) and UEA(-) stem cells (Red stars).

828 (**B**) The average % of UEA(-) stem cells that fall into the previously defined cell-cycle bins:
829 (Negative $G_0/G_1/G_2$; $G_1$ licensed; S-phase; $S/G_2$ phase; N=68 crypts).

830 (**C**) Representative flow cytometry profiles of (**i**) isolated $Lgr5^{Hi}$ intestinal stem cells showing
831 DNA-bound Mcm2 and DNA content (2ndry only control samples are shown); (**ii**) cells with a
832 2N ($G_1$) DNA content were selected and the DNA-bound Mcm2 is shown (left panels); their
833 Ki67 staining was then compared (right panels). (iii) The frequency distribution of mean
834 DNA-bound Mcm2 intensities for Mcm2(+) cells in $G_1$ cells is displayed. Hypothetical
835 scenarios for model frequency distributions of 'fast', 'slow' and 'no' licensing are displayed.
836 The profile for intestinal stem-cells is most similar to a 'no loading' scenario.

837 (**D**) Comparison of DNA-bound Mcm2 content of Lgr5(+) and Lgr5(-) $G_1$ cells and of cells in
838 very early S-phase.

839 (**E**) Label retaining '+4' cells were visualised using a pulse-chase protocol in H2B-GFP mice
840 (Supplementary Figure 4). A representative image of a crypt base is displayed highlighting a
841 label retaining (+4) cell (white arrow) that is GFP(+) UEA(-), and is distinct from label
842 retaining Paneth cells (GFP(+), UEA(+)).

843 **(F)** Representative images of H2B-GFP label-retaining cells in extracted intestinal crypts
844 stained with Hoechst (Blue) and an antibody against Mcm2 (Red). H2B-$GFP^{Hi}$ cells (bright
845 Green) represent Paneth cells and +4 cells, and H2B-$GFP^{Low}$ cells (Faint Green) represent
846 daughter cells that have diluted H2B-GFP content as a result of cell division.

847 (**G**) Quantification of the mean DNA-bound Mcm2 intensities in $GFP^{Hi}$ label retaining (LR) and
848 $GFP^{low}$ daughter cells compared with the total cell population (all cells). Displayed are the
849 mean +/- SEM (N=20 crypts).

850

851 **Figure 5. Contribution of the stem-cell niche to cell-cycle dynamics**

852 (**A**) Representative image of an extracted intestinal organoid stained with Hoechst (Blue),
853 Phalloidin (Green) and an antibody against Mcm2 (Red).

854 (**B**) Representative flow cytometry profiles from cells isolated from organoids (left) or from
855 intestinal tissue (right). Displayed is the quantification of DNA-bound Mcm2 content of $G_1$
856 cells (**i**). The percentage of fully licensed cells is also shown. The frequency distribution (ii) of
857 mean DNA-bound Mcm2 intensities for Mcm2(+) cells within $G_1$ cells for organoids and
858 intestinal crypts are displayed.

859 (**C**) Representative flow cytometry profiles of isolated organoid epithelial cells quantifying
860 Ki67 (**i**) and DNA-bound Mcm2 (**ii**) against DNA content or the comparison of DNA-bound
861 Mcm2 vs Ki67 (**iii**) Displayed is a representative plot from organoids grown in ENR media
862 alongside epithelial cells from isolated crypts (iv) (**See also S5 Figure A**).

863 (**D**) Representative flow cytometry profiles of isolated organoid epithelial cells grown in ENR
864 (control) and treated with the EGFR inhibitor Gefitinib, for the indicated times (**i-iii**). After 4
865 Days in Gefitinib, organoids were reactivated by removal of the Gefitinib and re-addition of
866 fresh growth factors for 2 days (**iv**). Displayed are profiles comparing DNA-bound Mcm2 vs
867 Ki67 (Top panels) or total Mcm2 content (Bottom panels).

868 (**E**) Representative flow cytometry profiles of isolated organoid epithelial cells grown in ENR
869 or ENR-CV media for 6 days comparing DNA-bound Mcm2 vs Ki67 content.
870
871 (**F**) Representative flow cytometry profiles from extracted cells isolated from organoids
872 treated with ENR or ENR-CV for indicated time periods. Displayed is the comparison of DNA-
873 bound Mcm2 vs Ki67 content.
874
875 (**G**) Organoids in ENR-CV media were treated with Gefitinib (EGFi) for 1 day and were 're-
876 activated' by fresh addition of ENR-CV for a further day. Representative flow cytometry
877 profiles of isolated organoid epithelial cells are shown comparing DNA-bound Mcm2 vs Ki67
878 content.
879

880 **Figure 6. Model of Origin licensing dynamics in intestinal epithelial cells**

881 In a normal cell-cycle, Mcms are expressed ubiquitously in all stages. The licensing of DNA
882 with MCM2-7 occurs in late M and throughout $G_{1,}$ when a cell receives a stimulus to commit
883 to the cell cycle. As DNA is replicated during S-phase, MCM2-7s are displaced from DNA and
884 are prevented from relicensing in $G_2$. During terminal differentiation, MCM2-7 are not
885 actively transcribed and the proteins are gradually lost in post-mitotic cells. However, after
886 the final mitotic division, cells make a binary decision never to license their DNA, even
887 though the protein is still present. Mcm proteins then degrade slowly, where cells enter a
888 terminally differentiated state (deep $G_0$). Alternatively, cells can exit mitosis, not relicense
889 their DNA but maintain proliferative markers and disengage from the cell cycle for some
890 time (shallow $G_0$). Two major classes of intestinal stem cells exist: 'Active' stem cells,
891 engaged with the cell-cycle, and reserve, quiescent Label Retaining Cells. Label retaining
892 cells are in a state of 'deep' quiescence, and do not contain MCM2-7 because they have
893 disengaged from the cell cycle for some time. In this study, we show that most 'Active'
894 Lgr5(+) stem cells reside in an unlicensed state, but contain MCM2-7 proteins. These cells
895 reside in a shallow-$G_0$' until they make a proliferative fate decision, enter the cell-cycle and
896 license. This provides an explanation for the elongated cell-cycle of Intestinal stem cells:
897 They reside in a partial resting state where they may be able to respond to niche cues to
898 divide. This therefore may constitute a unique mechanism to control stem cell numbers.

## Supplementary Figure Legends

### S1 Figure. Image analysis

(**A**) Maximum intensity projections of intestinal tissue revealing intestinal crypts and villi (left panels). Individual X-Y sections are also shown to reveal the epithelium (right panels). Tissue was stained with Phalloidin (Green) and Hoechst (Blue) and an antibody against Mcm2 (Red).

(**B**) Image analysis work-flow.

(**C**) Representative image of an extracted isolated crypt 1 hour after an EdU pulse (Green) stained with Hoechst (Blue) and an antibody against Mcm2 (Red).

(**D**) Detection of nuclei in the crypt in panel A in 3D. Nuclei were detected in 3D using segmentation tools in Imaris. Detection was validated visually or each individual crypt.

(**E**) Segmentation of the region of interest defined by nuclei detection in panel B.

(**F**) A distance transform was performed in Imaris to measure the distance of each nucleus to a reference nucleus at the crypt base. Visual representations of distances divided into different bins are displayed (Green, 0-10µm; Yellow, 10-20 µm; Red, 20-30µm; Blue, 30-40µm; Magenta, 40-50µm).

(**G**) Representative 3D quantification of the crypt in panel A shows the distance from the crypt base (X-axis), DNA-bound Mcm2 (Y-axis) and EdU incorporation (Z-axis).

(**G**) Quantification of Mcm2 and EdU intensities in cell-cycle phases shown in Figure 3A. Displayed are the mean intensities for DNA-bound Mcm2 and EdU for each cell-cycle phase (N=10 cells).

920 **S2 Figure. Clonal cell-cycle patterns in the intestinal epithelium**

921 **(A**) Representative section through an extracted crypt after a 1 hour EdU pulse (Green) and
922 stained with Hoechst (Blue) and an antibody against Mcm2 (Red). Discrimination of cell-
923 cycle staging using DNA-bound Mcm2 and EdU incorporation patterns allows visualisation of
924 clonal cell-cycle field effects revealing many neighbouring cells with similar DNA-bound
925 Mcm2 and DNA replication patterns. These clones may represent lineages of from single
926 cells that progress through the cell cycle at the same rate.

927 (**B**) Representative image of an isolated crypt in which surface rendering was performed on
928 all nuclei and colour codes applied to reflect cell-cycle stage. Representative cell-cycle
929 distributions for isolated Ki67(+), Lgr5(+) and Lgr5(-) intestinal epithelial cells are shown.

930 (**C**) Representative cell-cycle distributions for isolated Ki67(+), Lgr5(+) and Lgr5(-) intestinal
931 epithelial cells. The average of each cell-cycle phase is displayed for duplicate isolations.

932 (**D**) Nuclear volumes were rendered for individual nuclei in whole intestinal crypts isolated 1
933 hour after labelling with EdU. Image shows nuclei (Blue), EdU (Green) and licensed Mcm2
934 (Red). Maximum intensity projections of the original image are displayed at the top and
935 corresponding rendered nuclei at the bottom. Nuclear surfaces were colour-coded
936 according to cell-cycle states: Blue, unlicensed; Red, Licensed $G_1$; Yellow, S-phase; Green,
937 Late-S/$G_2$. Nuclear volumes were measured for all nuclei in representative crypts (N=3).
938 Unlicensed (N=368); $G_1$ (N=104); S-phase (N=41); Late-S/$G_2$ (N=70) and the distance of cells
939 from the crypt base were binned into 10µm intervals. Known parameters of the nuclear
940 volume for known cell-cycle stages (Figure 3B) are overlaid.

941

942 **S3 Figure. Ki67 expression along the crypt-villus axis**

943 **(A**) A representative isolated crypt 1 hour after labelling with EdU (Green) and stained with
944 an antibody against Ki67 (magenta)

945 (**B**) Quantification of the distribution of Ki67(+) cells along the crypt axis. Cells were binned
946 into four groups: Negative (Ki67(-), EdU(-)); Ki67(+), EdU(-); Ki67(+), EdU(+) and Ki67(-),
947 (EdU(+) and by their distance from the crypt base. Data is displayed as the average
948 percentage of a particular cell subtype, per distance bin. Data is displayed as Mean +/- SEM.
949 Data from 75 crypts is displayed, N = 14,264 cells.

950

951 **S4 Figure. H2B-GFP labelling strategy**

952 (**A**) Labelling strategy. H2B-GFP expression was induced in all intestinal epithelial cells in
953 H2B-GFP mice by administration of doxycycline for 7 days. After complete labelling,
954 doxycycline was removed and mice rested for 4-7 days. During this chase period, the
955 majority of H2B-GFP(+) cells are lost by label dilution due to cell division and upward
956 migration.

957 (**B**) Representative images of whole-mount sections of H2B-GFP expressing small-intestinal
958 tissue after a 7day labelling period. Maximum intensity images show fully labelled crypts
959 and villi.

960 (**C**) A representative image of an isolated villus fragment isolated 7 days after last doxycyclin
961 administration, stained with Hoechst (Blue) and an antibody against GFP (Red). Image shows
962 the accumulation of GFP(+) label retaining cells at the villus tip.

963 (**D**) A vibratome section of H2B-GFP epithelium after a 7-day chase period. Tissue was
964 stained with Hoechst (Blue) and an antibody against GFP (Red). The unamplified GFP signal
965 (white) is only detectable in infrequently dividing cells such as Paneth cells or label retaining
966 +4 cells. Antibody-mediated amplification of the GFP signal allows visualisation of lower GFP
967 expression in daughter cells persisting in the crypt.

968 (**E**) Quantification of the mean GFP intensity for all cells along the crypt-villus axis 7 days
969 after final doxycycline treatment. The majority of GFP(+) cells reside within the stem cell
970 compartment 0-40µm from the crypt base.

971 (**F**) Extraction does not affect H2B-GFP expression. Representative image of a fully induced,
972 extracted H2B-GFP (Green) crypt stained with an antibody against Mcm2 (Red).

973 **S5 Figure. Manipulation of the stem cell niche can artificially induce shallow-$G_0$**

974 (**A**) Representative flow cytometry profile of extracted epithelial cells isolated from
975 organoids in ENR media. The displayed image is the same profile displayed in Figure 5C. The
976 populations in boxed regions 1-7 are overlaid onto the Mcm2 and Ki67 cell-cycle profiles.

977 (**B**) Representative images of Lgr5-GFP organoids treated with ENR or ENR-CV. In ENR-CV
978 treated organoids, the majority of cells express Lgr5.

979 (**C**) Representative flow cytometry profiles from extracted cells isolated from organoids
980 treated with Valproic acid or Chir99021 alone for indicated time intervals.

981 (**D**) Representative flow cytometry profiles from extracted cells isolated from organoids
982 treated with DAPT for indicated time intervals.

983 (**E**) Model for the unique cell-cycle characteristics of organoid epithelial cells.
984 Normal, highly proliferative cells, express Ki67 and Mcm2 protein that is not DNA-bound (**1**).
985 During a normal cell-cycle, cells are activated from this shallow-$G_0$ state, and rapidly license
986 origins (**2**). Mcms are subsequently displaced during DNA replication (**3**) and remain
987 unlicensed through $G_2$ (**3**). Inhibiting EGFR causes highly proliferative cells ($Ki67^{hi}$) to arrest
988 in shallow-$G_0$ with maintained Mcm2 protein expression. Prolonged EGFRi treatment causes
989 transition into an intermediate state of $G_0$ accompanied by loss of Ki67 expression ($Ki67^{lo}$),
990 but maintenance of MCM2-7 protein expression (**4**). Induction of terminal differentiation by
991 inhibition of Notch signalling is associated with a terminal loss of MCM2-7 proteins, and
992 entry into deep-$G_0$ (**5**). HDAC inhibition (HDACi) or Notch activation induces a unique subset
993 of $Ki67^{lo}$ shallow-$G_0$ cells to license origins independently of Ki67 expression (**6**). We suggest
994 that the unique cell population observed upon ENR-CV / ENR-V treatment may be a reserve
995 subset of stem cells that express Lgr5 and start expressing MCM2-7 and enter shallow-$G_0$
996 from deep-$G_0$. These cells have unique cell cycle characteristics, and can immediately license
997 origins independently of Ki67 expression (6→2→3).

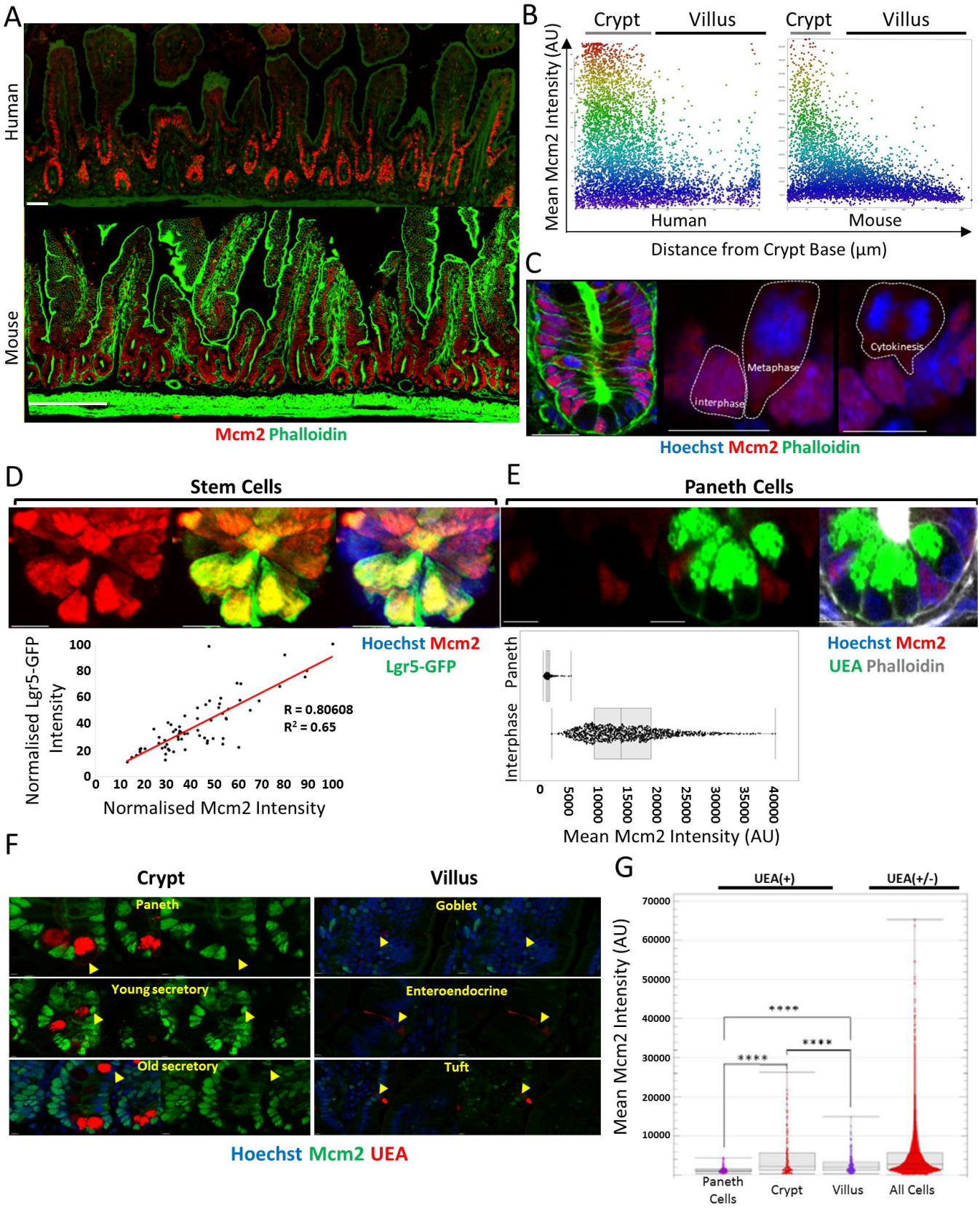


Carroll et al., Figure 1

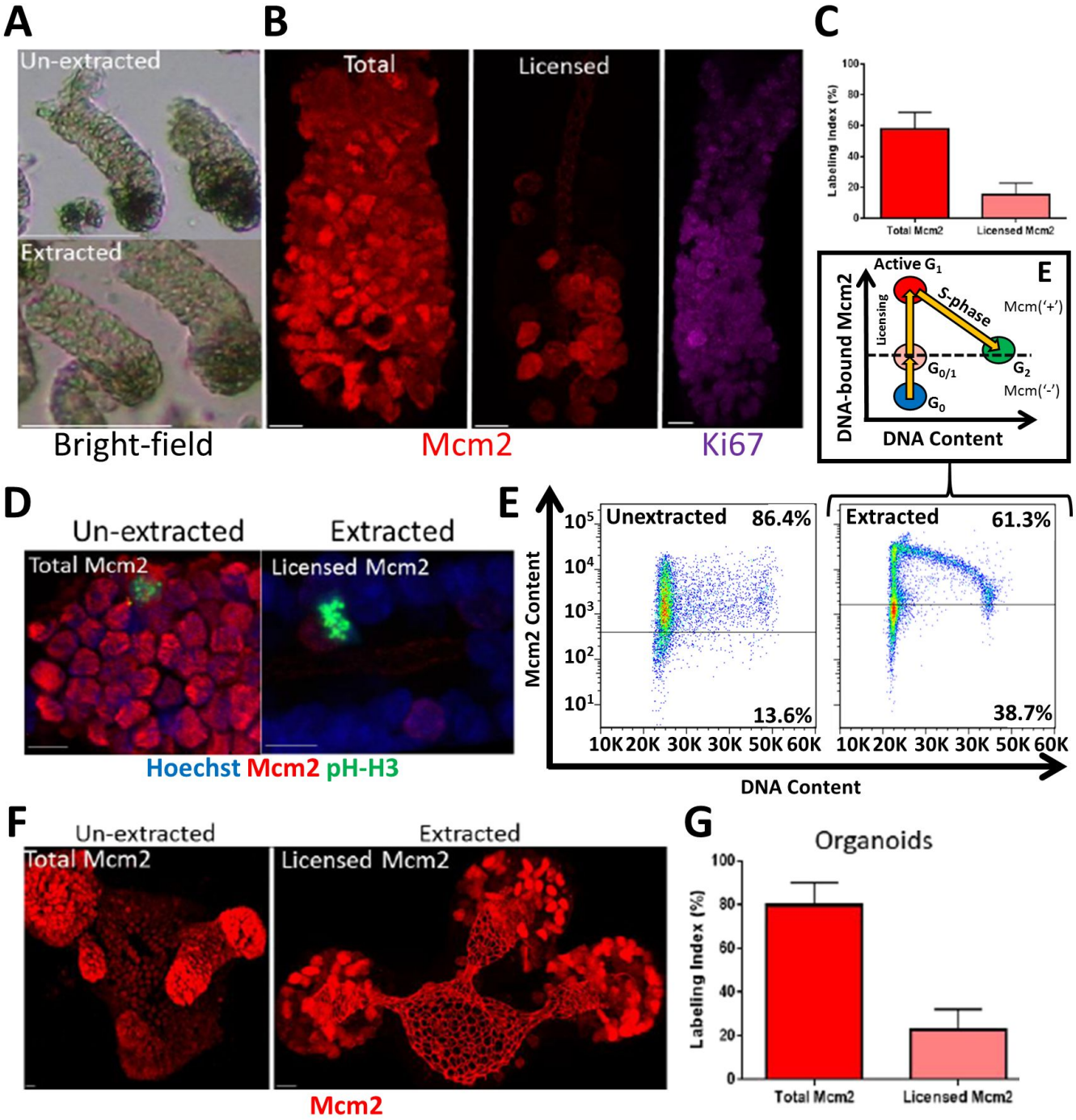


Carroll et al., Figure 2

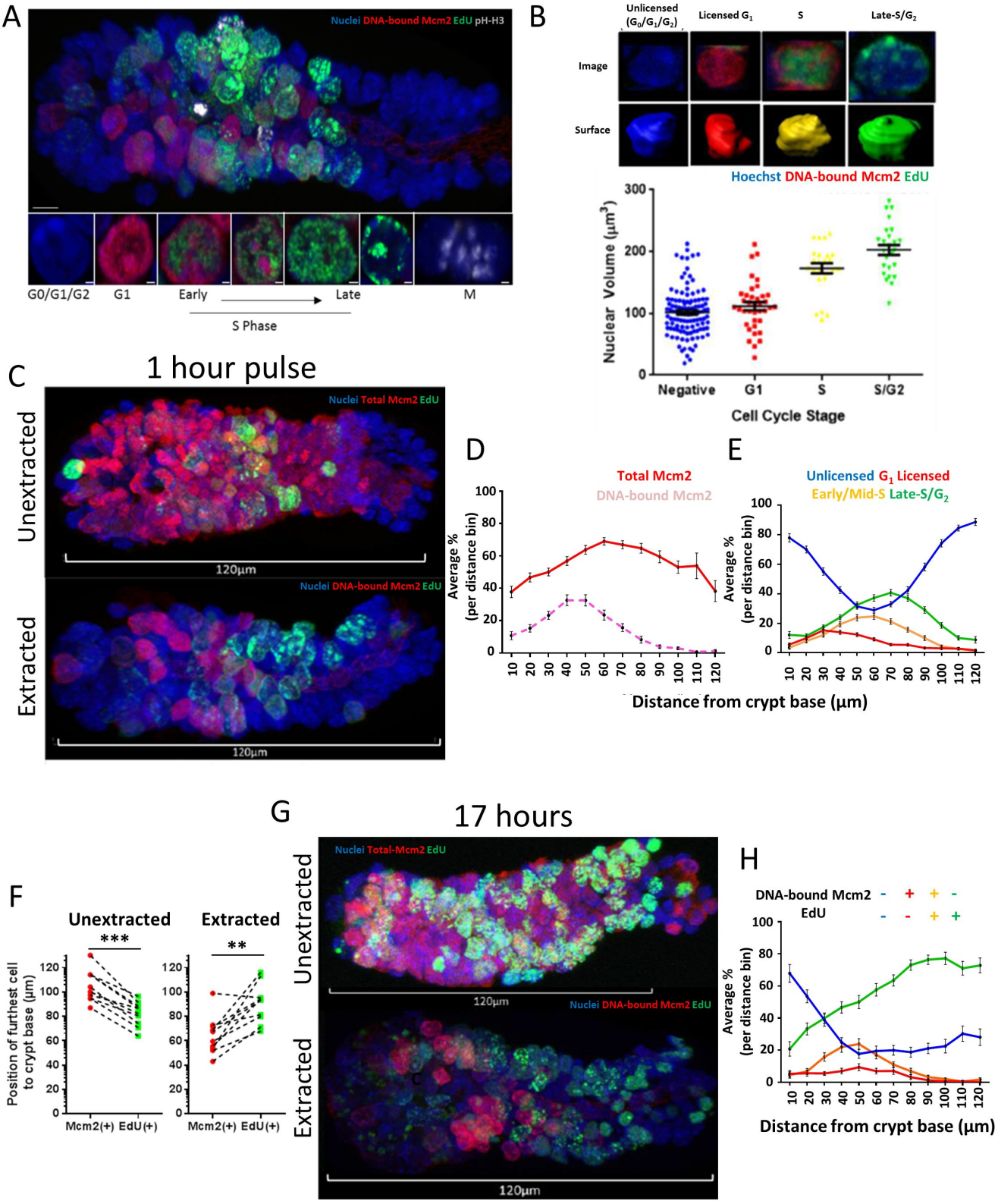


Carroll et al., Figure 3

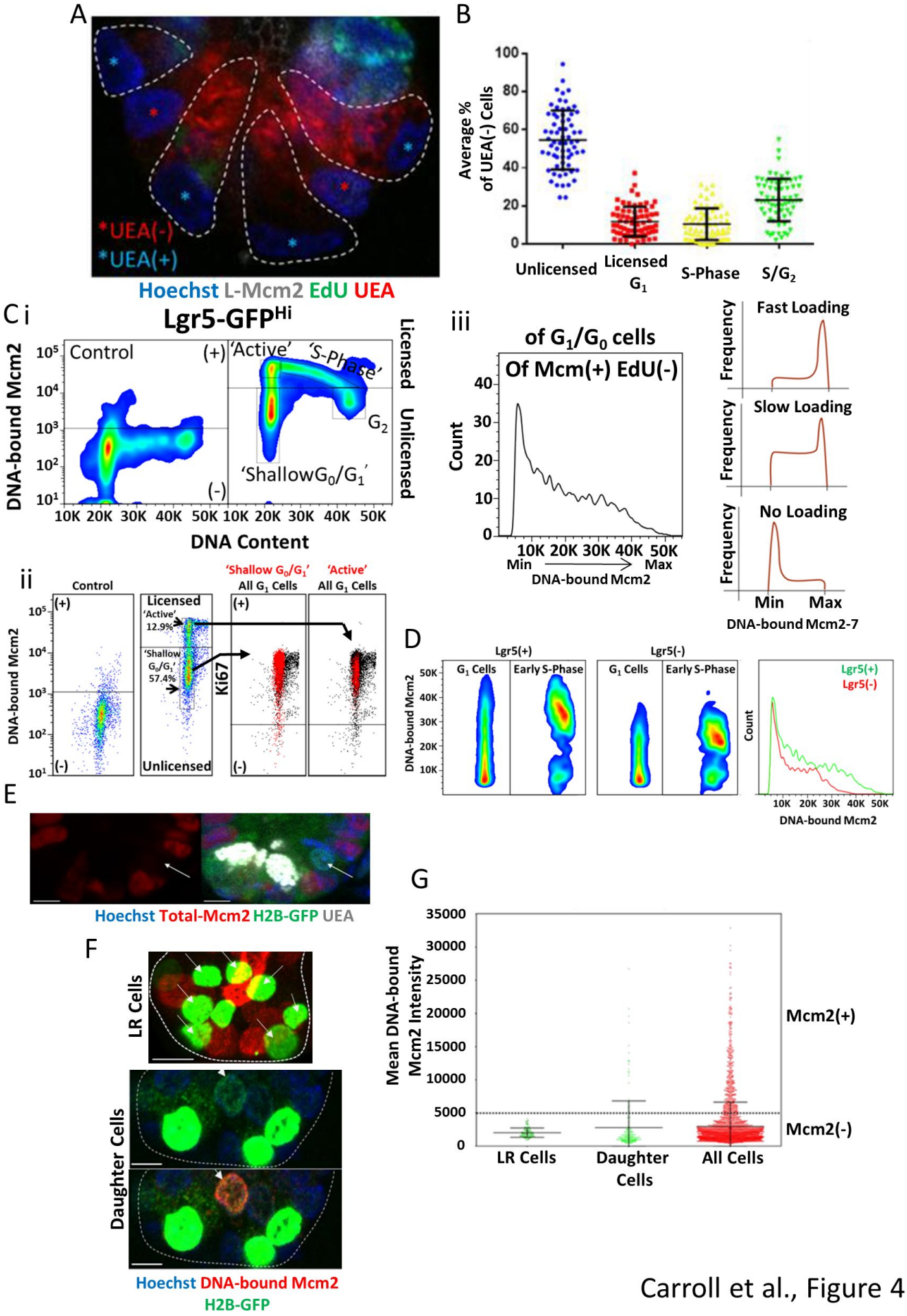


Carroll et al., Figure 4

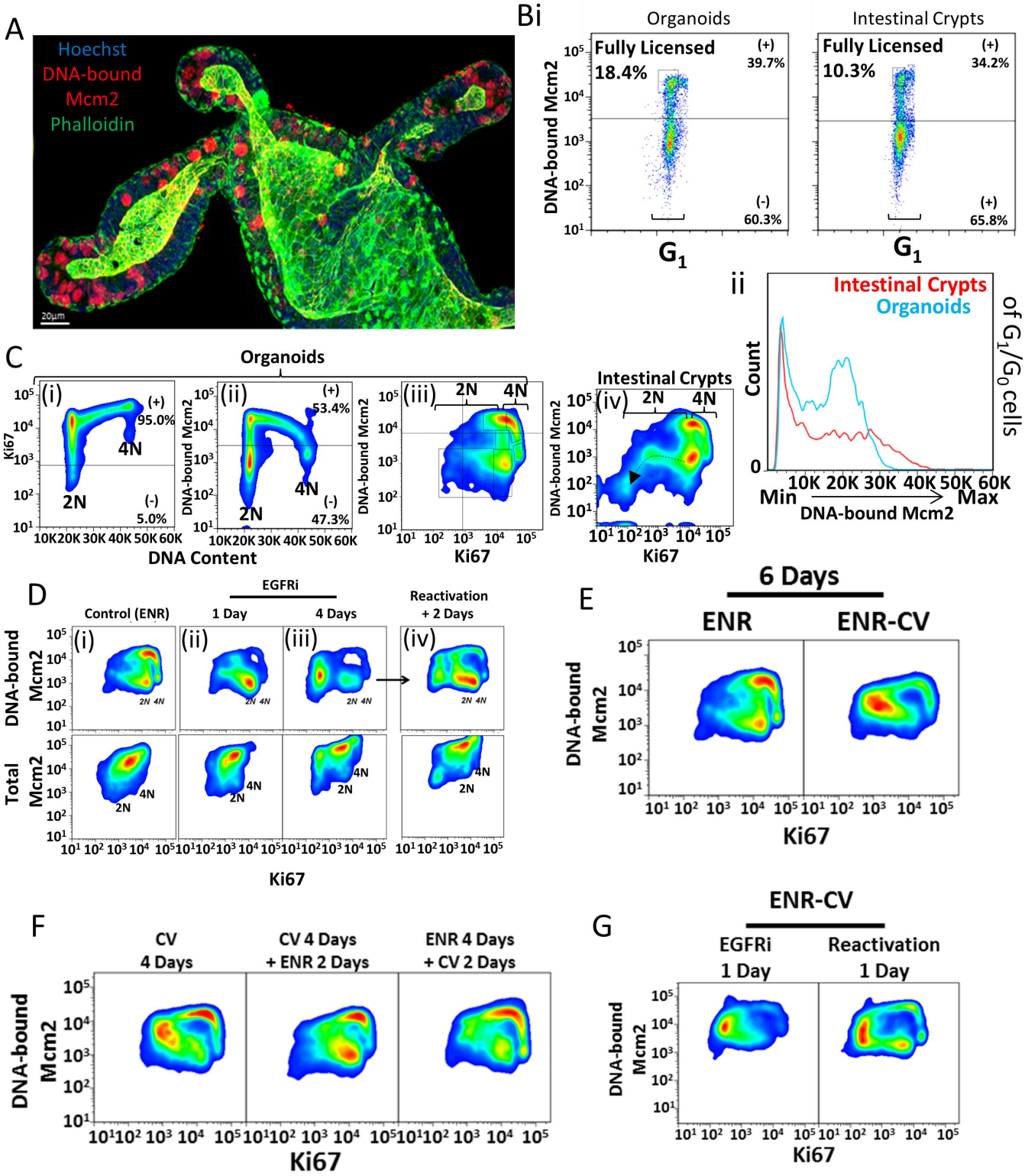


Carroll et al., Figure 5

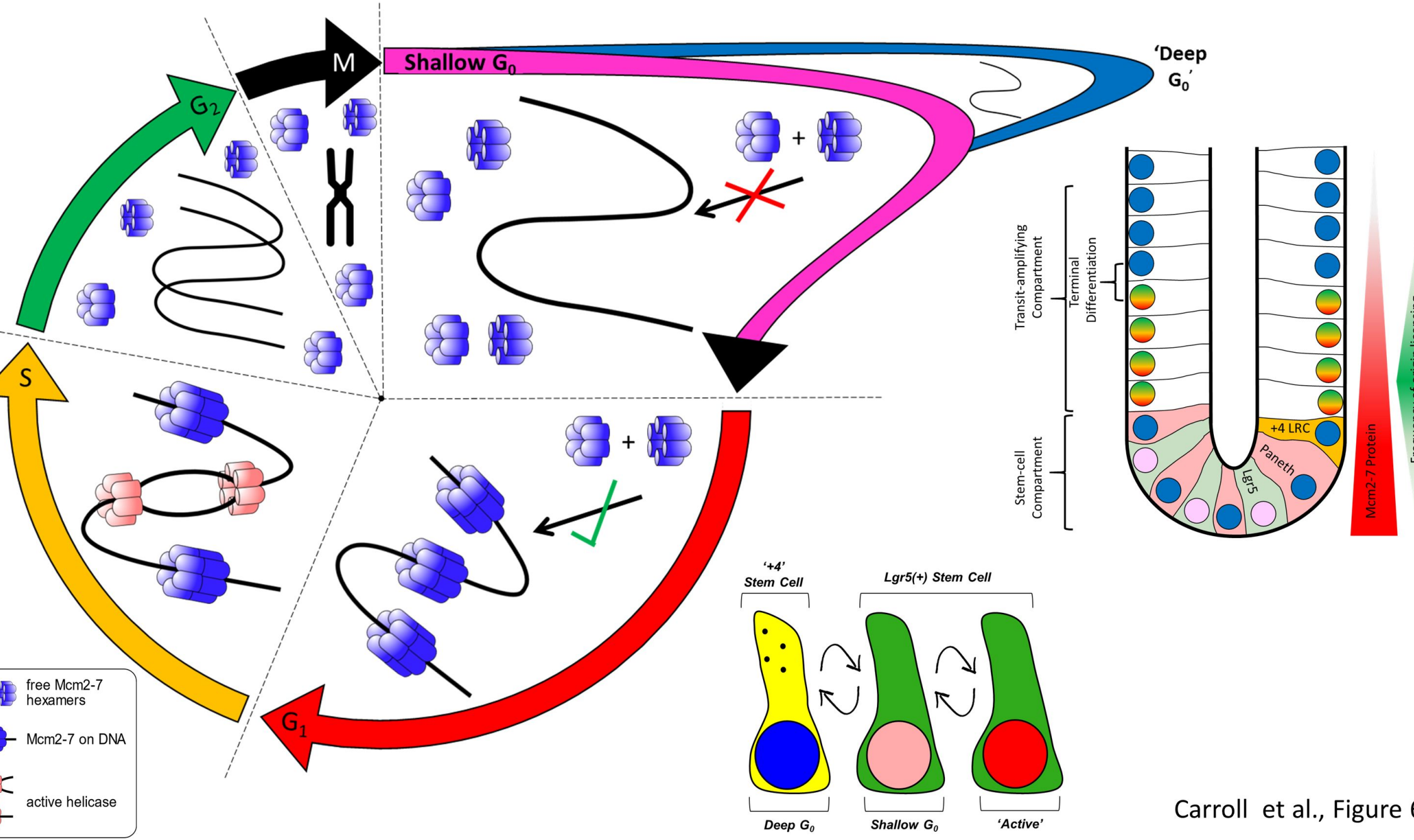


Carroll et al., Figure 6

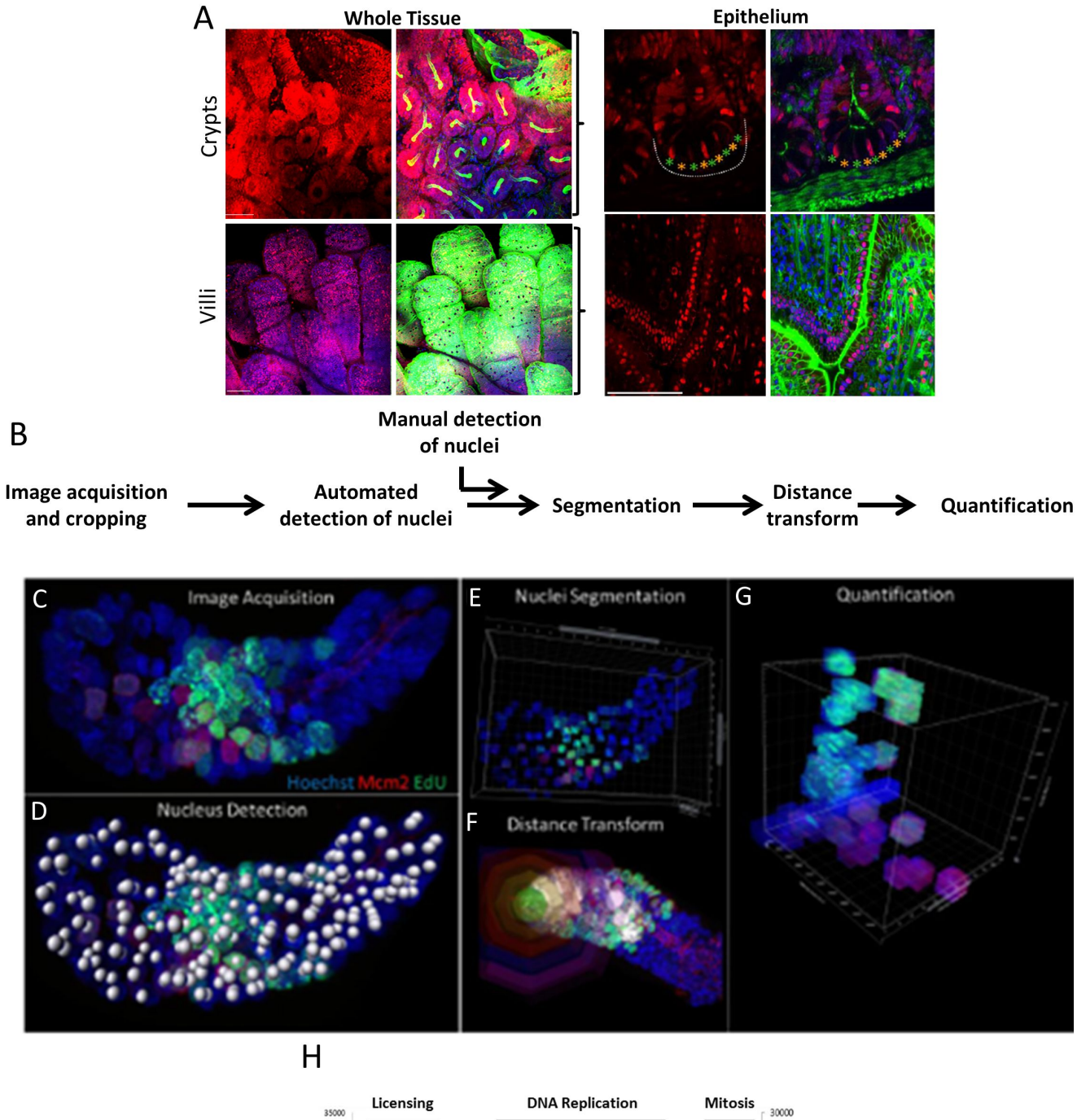


Carroll et al., S1 Figure

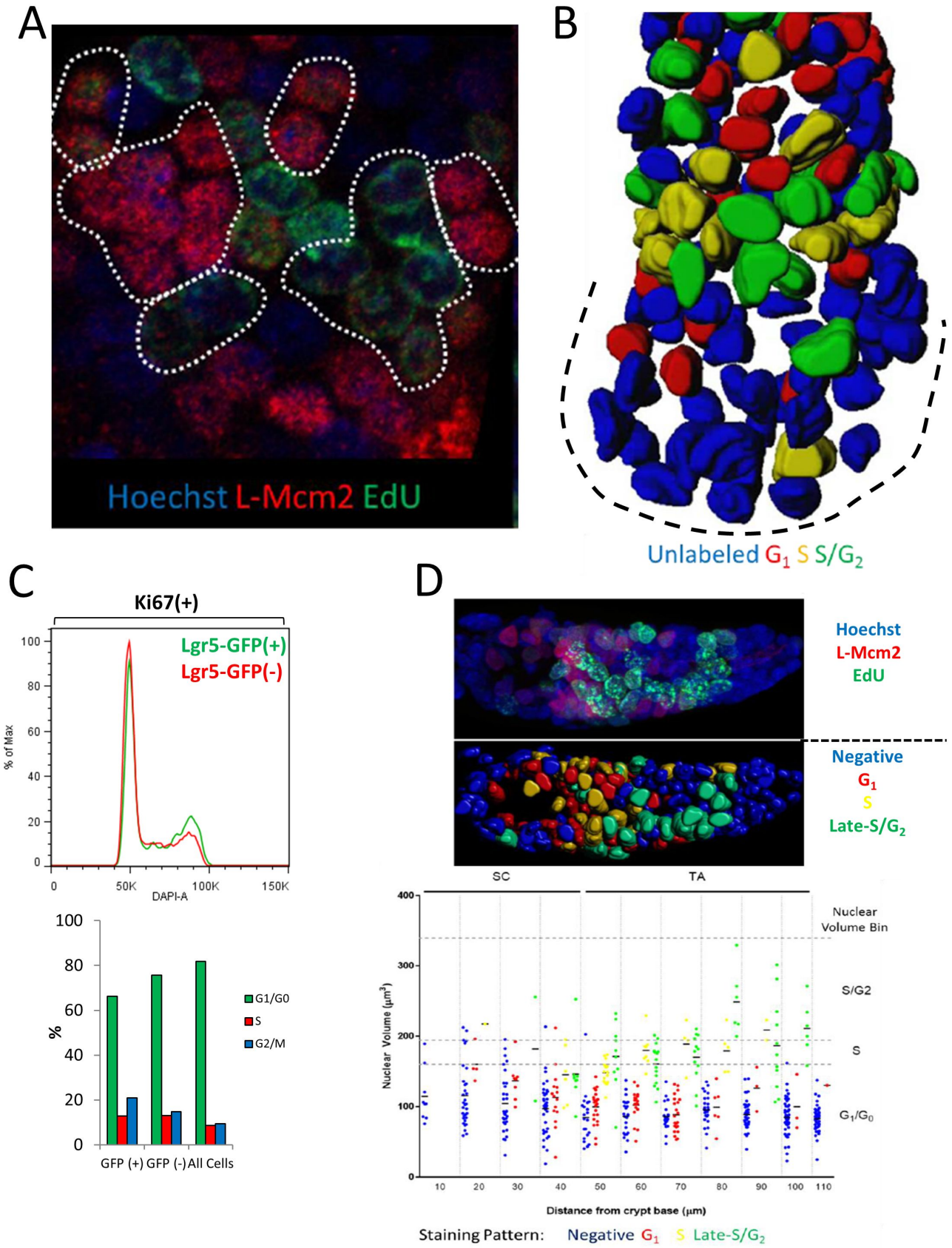


Carroll et al., S2 Figure

A

1 Hour pulse

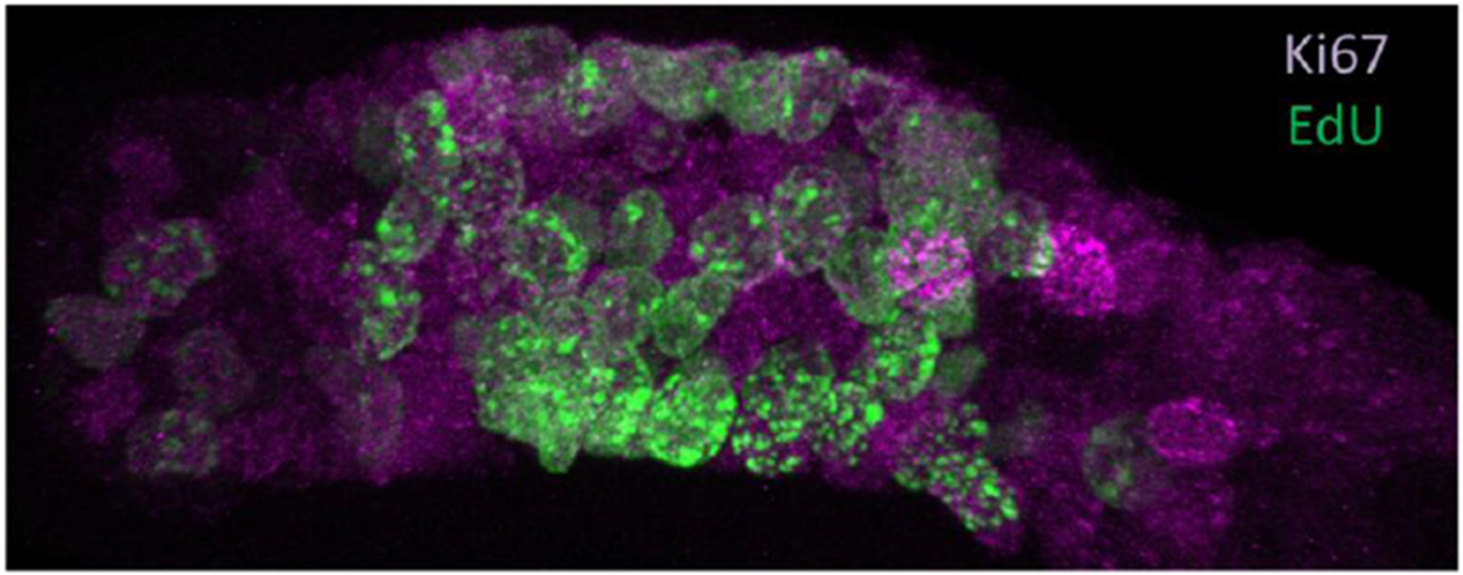


B

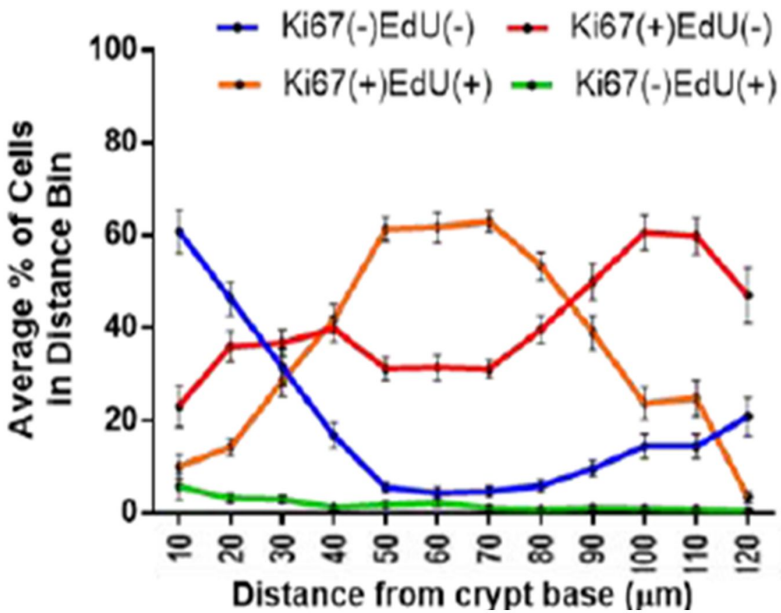


Carroll et al., S3 Figure

A

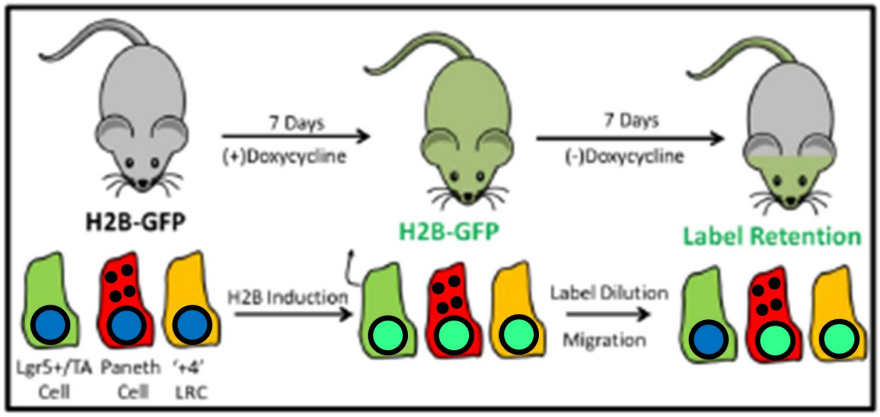


B

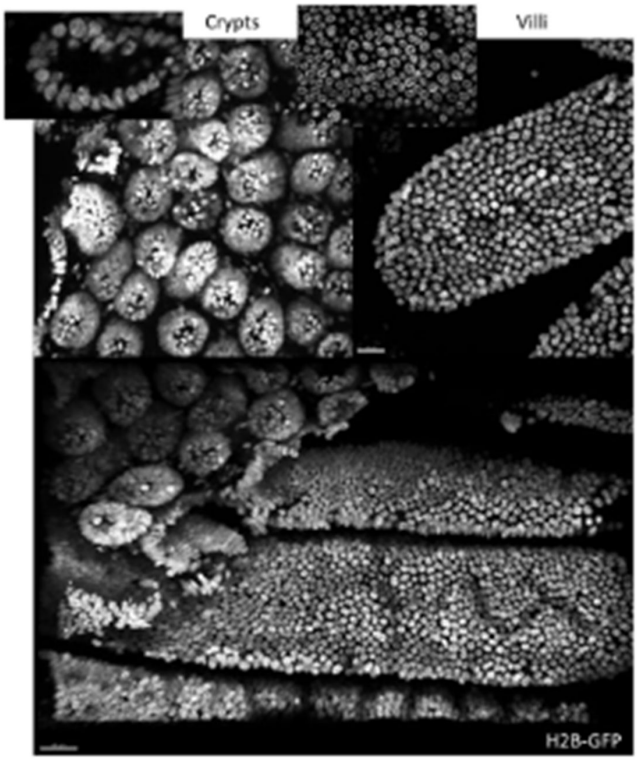


7 Days Induction

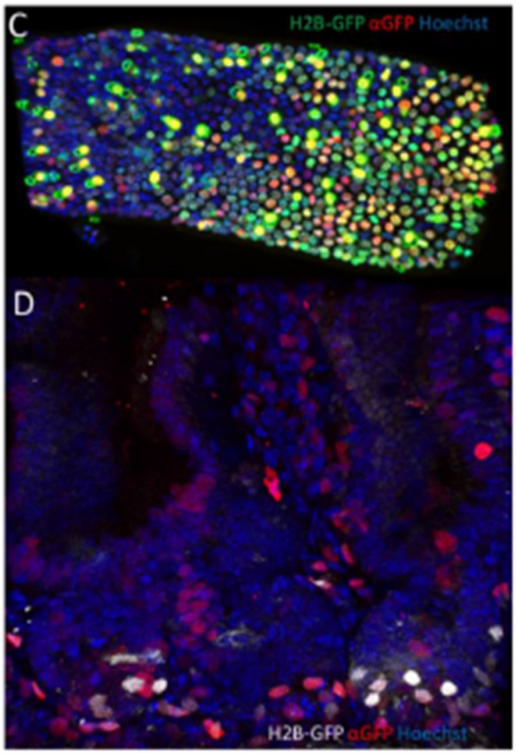


7 Days Chase

E

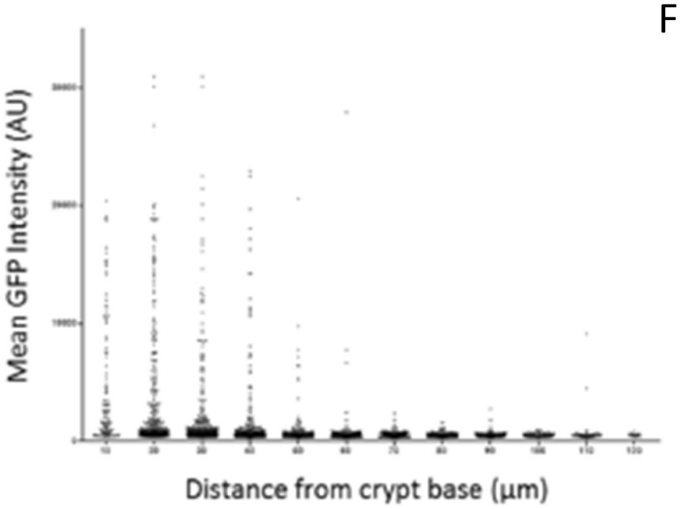


F

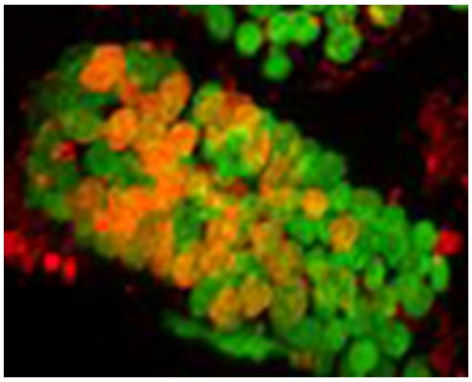

DNA-bound Mcm2 H2B-GFP

Carroll et al., S4 Figure

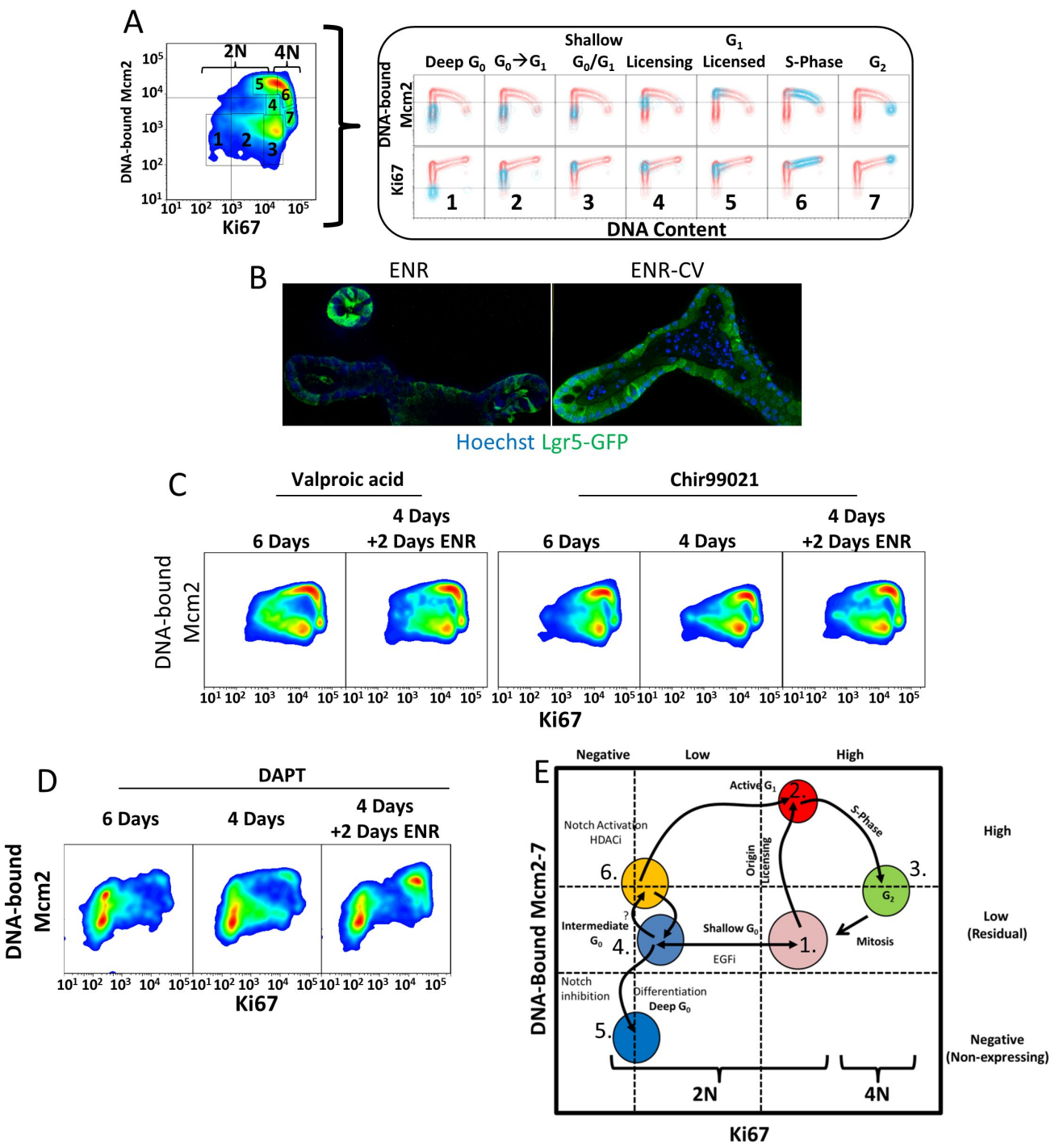


Carroll et al., S5 Figure